Entanglement Phase Transition Due to Reciprocity Breaking without Measurement or Postselection

Gideon Lee,[1,*] Tony Jin,[1] Yu-Xin Wang (王语馨),[1] Alexander McDonald,[2] and Aashish Clerk[1]

[1] *Pritzker School of Molecular Engineering, The University of Chicago, Chicago, Illinois 60637, USA*

[2] *Institut Quantique and Département de Physique, Université de Sherbrooke, Sherbrooke, Québec J1K 2R1, Canada*

(Received 6 September 2023; accepted 20 December 2023; published 31 January 2024)

Despite its fully unitary dynamics, the bosonic Kitaev chain (BKC) displays key hallmarks of non-Hermitian physics, including nonreciprocal transport and the non-Hermitian skin effect. Here, we demonstrate another remarkable phenomena: the existence of an entanglement phase transition (EPT) in a variant of the BKC that occurs as a function of a Hamiltonian parameter g and which coincides with a transition from a reciprocal to a nonreciprocal phase. As g is reduced below a critical value, the postquench entanglement entropy of a subsystem of size l goes from a volume-law phase, where it scales as l, to a *supervolume*-law phase, where it scales like lN, where N is the total system size. This EPT occurs for a system undergoing purely unitary evolution and does not involve measurements, postselection, disorder, or dissipation. We derive analytically the entanglement entropy out of and at the critical point for the cases of $l = 1$ and $l/N \ll 1$.

DOI: 10.1103/PRXQuantum.5.010313

I. INTRODUCTION

Recent years have seen intense efforts focused on understanding entanglement dynamics in many-body quantum systems with nonunitary evolution. It has been found that for chaotic systems, measurements can trigger a novel phase transition from an entangled phase to a disentangled phase, a phenomenon dubbed a measurement-induced phase transition (MiPT) [1–10]. While these models provide fertile ground for the development of rich theoretical ideas at the intersection of statistical physics and quantum information [11–17], direct experimental observation of MiPTs can be extremely challenging, as this requires access to the full conditioned evolution [18] (although note that alternative strategies based on quantities other than entanglement have been studied both theoretically [19–26] and experimentally [21,27]).

While MiPT is typically studied in systems where entanglement must be averaged over different random trajectories corresponding to distinct measurement outcomes, recent work has shown that entanglement phase transitions (EPTs) can also occur without any stochasticity, in systems evolving under a non-Hermitian Hamiltonian [28–31]. There is a direct connection to MiPT, as non-Hermitian dynamics are naturally interpreted as arising from measurement dynamics where one postselects on a specific set of null measurement outcomes. Of particular interest here are studies of EPT in non-Hermitian models exhibiting nonreciprocity (e.g., directional systems where hopping to the right is much stronger than to the left). Kawabata *et al.* [29] have studied an EPT in such a system (two coupled fermionic Hatano-Nelson [32,33] chains) from volume-law to area-law entanglement scaling. They have found that the transition coincides with the transition between a reciprocal and a nonreciprocal phase. The latter could be directly witnessed by the non-Hermitian skin effect (NHSE), a phenomenon occurring in the nonreciprocal phase where all modes localize under open boundary conditions [32–41]. Despite this striking correspondence, one could still view the EPT transition here as being measurement driven, as the strength of nonreciprocity is directly tied to the strength of a postselected measurement.

Taking inspiration from these previous studies, in this work we ask whether an EPT can occur without any stochasticity *and* without any need for measurements (postselected or not). Similar to Ref. [29], we consider a translationally invariant model that exhibits a transition between reciprocal and nonreciprocal phases (with the latter exhibiting the NHSE). In contrast to that work, our model has a *fully Hermitian* Hamiltonian and unitary

*gideonlee@uchicago.edu

evolution and there is no need for any kind of measurement, postselection or dissipation. Our setting is Hermitian quadratic many-body bosonic Hamiltonians that do not conserve the particle number. Such models can exhibit nonreciprocity: despite being fully unitary, the dynamics can nonetheless exhibit directionality at the level of the equations of motion for quadratures [37,42–44]. Given that such models can exhibit nonreciprocity transitions, can they also exhibit entanglement transitions despite the lack of any connection to measurements?

We find that the answer to this question is, surprisingly, yes. Our main result is to present the first instance of an EPT in a nondisordered bosonic system under purely unitary dynamics. We stress that this EPT requires *no postselection whatsoever*. Furthermore, as this model contains neither randomness nor measurements, one can unambiguously attribute this EPT to reciprocity breaking. Our model of interest is a variant of the the bosonic Kitaev chain (BKC) model introduced in Ref. [37]. By tuning a Hamiltonian parameter g, the BKC undergoes a phase transition from a phase where the dynamics of the q and p quadratures are nonreciprocal to a phase where they are reciprocal. At long times after a quench, the reciprocal phase is characterized by a volume law for the entanglement entropy (EE) of a subsystem of size l, i.e., it scales linearly with l. On the other hand, the nonreciprocal phase has even stronger entanglement growth. It is characterized by what we call a *supervolume* law: the EE of a subsystem of size l scales as lN, where N is the total system size. Hence, if take a symmetric bipartition, the EE grows as N^2. These forms of behavior are in stark contrast with Ref. [29], which has also tied entanglement and reciprocity transitions but has found that nonreciprocity is detrimental to entanglement generation, leading to area-law behavior (see Sec. III). We also note that our results (for an unmeasured system) are distinct from the behavior of explicitly monitored quadratic bosonic systems, which do not exhibit an EPT [45,46]. In addition to being of fundamental interest, our setup is also attractive for experiments. The absence of any requirement for measurements or postselection greatly simplifies implementation, while the Hermitian bosonic pairing terms that we require can be implemented in a variety of different platforms (they correspond to parametric drives or parametric down-conversion).

The remainder of this paper is organized as follows. In Sec. II, we recall the basic phenomenology of the BKC in both nonreciprocal and reciprocal phases. In Sec. III, we present a numerical demonstration of the EPT. In Sec. IV, we study analytically, in depth, the special minimal-bipartition case $l = 1$ and show that it already captures the essential features of the EPT. In Sec. V, we extend the $l = 1$ results to the $l/N \ll 1$ case by relying on a local-thermalization hypothesis toward a generalized Gibbs ensemble (GGE). Finally, in Sec. VI, we conclude and discuss future directions.

II. MODEL

The BKC describes bosonic modes on a one-dimensional (1D) lattice that are coupled by hopping and pairing terms on each nearest-neighbor bond. The Hamiltonian is

$$\hat{H} = \frac{1}{2}\sum_{j=1}^{N-1}\left((g+iw)\hat{a}_{j+1}^{\dagger}\hat{a}_j + i\Delta\hat{a}_{j+1}^{\dagger}\hat{a}_j^{\dagger} + \text{H.c.}\right), \quad (1)$$

where N is the total number of sites, $\hat{a}_j$ are bosonic operators, $[\hat{a}_i, \hat{a}_j^{\dagger}] = \delta_{ij}$, and g, w, and Δ are real parameters of the model (see Fig. 1). We will call $\hat{\mathbf{r}} := (\hat{q}_1, \hat{p}_1, \ldots, \hat{q}_N, \hat{p}_N)^T$ the vector of quadrature operators, $\hat{q}_j := (\hat{a}_j + \hat{a}_j^{\dagger})/\sqrt{2}, \hat{p}_j := i(\hat{a}_j^{\dagger} - \hat{a}_j)/\sqrt{2}$.

Since $\hat{H}$ is quadratic, Gaussian states remain Gaussian under time evolution and are fully specified by their one-point function $\langle\hat{\mathbf{r}}\rangle$ and their $2N \times 2N$ covariance matrix $\sigma_{ij} = \langle\{\hat{\mathbf{r}}_i - \langle\hat{\mathbf{r}}_i\rangle, \hat{\mathbf{r}}_j - \langle\hat{\mathbf{r}}_j\rangle\}\rangle$. In the rest of this paper, we will fix the initial state to be vacuum, so that $\langle\hat{\mathbf{r}}\rangle = 0$ at all times. The equations of motion (EOMs) for σ close on themselves and are given by

$$\frac{d}{dt}\sigma = \Omega h\sigma + \sigma h\Omega^T, \quad (2)$$

where h is the bosonic Bogoliubov–de Gennes (BdG) $2N \times 2N$ matrix, defined through $\hat{H} = \hat{\mathbf{r}}^T h\hat{\mathbf{r}}$, and Ω is the symplectic matrix $\Omega := \bigoplus_{j=1}^{N}\left(\begin{smallmatrix}0 & 1\\ -1 & 0\end{smallmatrix}\right)$. Note that the dynamics are completely linear in σ.

The qualitative properties of the BKC are best understood by inspecting the Heisenberg EOMs of $\hat{\mathbf{r}}$:

$$\begin{aligned}\frac{d}{dt}\hat{q}_j &= \frac{w+\Delta}{2}\hat{q}_{j-1} - \frac{w-\Delta}{2}\hat{q}_{j+1} + \frac{g}{2}(\hat{p}_{j-1} + \hat{p}_{j+1}),\\ \frac{d}{dt}\hat{p}_j &= \frac{w-\Delta}{2}\hat{p}_{j-1} - \frac{w+\Delta}{2}\hat{p}_{j+1} - \frac{g}{2}(\hat{q}_{j-1} + \hat{q}_{j+1}).\end{aligned} \quad (3)$$

For $g = 0$ (i.e., purely imaginary hopping), these EOMs would describe independent nonreciprocal propagation of the q and p quadratures, with each having opposite directionality. This mimics the physics of two independent Hatano-Nelson chains [32,33].

We focus throughout in this work on the case $w > \Delta$ [47]. In this regime, the model is always dynamically stable for open boundary conditions (OBCs), while for periodic boundary conditions (PBCs) the system has a transition from stable to unstable as one goes from $\Delta < g$ to $g < \Delta$. The stability of this bosonic system for $g = 0$ can be conveniently understood in terms of amplification [37]: starting from a wave packet in the q quadrature localized on one edge, the wave packet will be amplified (damped) while propagating to the right (left) and

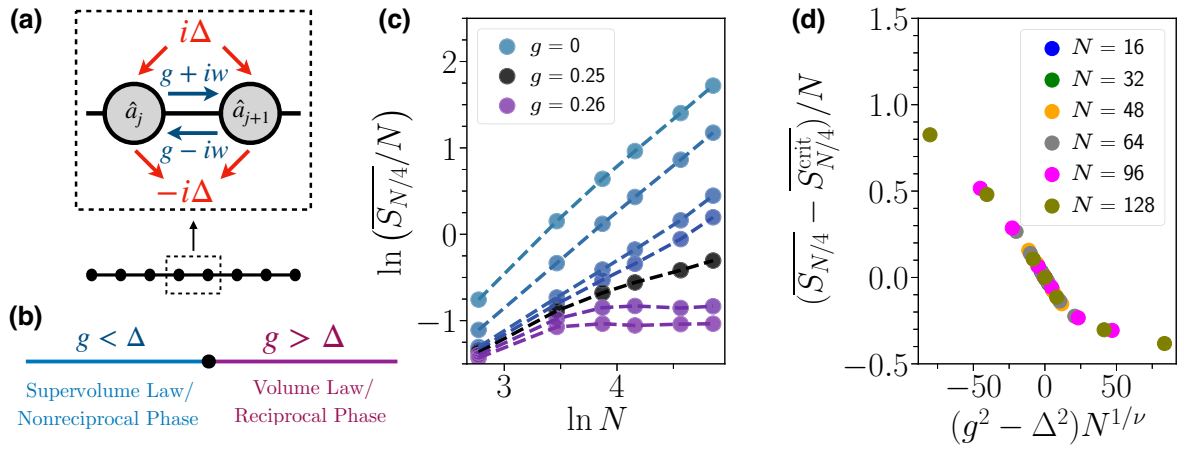

FIG. 1. (a) The schematic of a one-dimensional (1D) BKC lattice, with Hermitian hopping of amplitude $g + iw$ and pairing (two-mode squeezing) of amplitude $i\Delta$ on each bond [see Eq. (1)]. (b) The schematic of a phase diagram depicting supervolume-law and volume-law phases that arise as a function of g/Δ (with $g, \Delta < w$). For $g < \Delta$, the BKC exhibits the NHSE and has nonreciprocal dynamics leading to supervolume-law entanglement scaling (see the text), whereas for $g > \Delta$, the BKC is reciprocal and exhibits the usual volume law of free systems. (c) The log-log plot of the long-time-averaged EE for a subsystem formed by the leftmost $N/4$ sites, divided by system size. The circles are values from numerical simulation, while the dashed lines are simply a guide to the eye. Since the y axis is divided by N, a slope of 0 (greater than 0) indicates volume law (supervolume law). A clear transition is seen as g is increased above Δ. We fix $w = 1$ and $\Delta = 0.25$ and the values of g for the lines from blue to purple are 0, 0.2, 0.24, 0.245, 0.25, 0.255, and 0.26. (d) Scaling collapse of the long-time averaged EE for a subsystem of size $N/4$, with $\nu = 0.5$ in Eq. (9).

vice versa for the p quadratures. For PBCs, this amplification is unbounded, thus making the system unstable. In contrast, for OBCs, the amplification terminates at the edges, so that all average moments of the q quadratures are localized to the right and the p quadratures to the left. Adding a coupling g mixes the quadratures together; as they have opposite directionality at $g = 0$, this mixing diminishes nonreciprocity. As g increases, this mixing eventually prevents chiral amplification altogether, leading to a sharp transition from a *nonreciprocal* phase for $g < \Delta$ to a *reciprocal* phase for $g > \Delta$.

Another manifestation of this transition can be seen from the spectrum of the dynamical matrix $i\Omega h$, which exhibits the *non-Hermitian skin effect* (NHSE). This means that in the nonreciprocal phase, $g < \Delta$, for PBCs the spectrum of $i\Omega h$ winds around 0 in the complex plane, (i.e., the system is unstable), whereas the spectrum under OBCs collapses onto the real line (i.e., the system is stable). This is accompanied by the localization of all the OBC eigenmodes to the edges [34,48]. Conversely, in the reciprocal phase $g > \Delta$, the NHSE is absent—the spectrum is always real, regardless of the boundary conditions. We note that the spectral properties of $i\Omega h$ are in complete analogy with the spectral properties of the non-Hermitian BdG Hamiltonian presented in Ref. [29] where an EPT has been studied in coupled fermionic Hatano-Nelson chains. However, despite this similarity, we will show that the phenomenology in our Hermitian bosonic model is dramatically different. Given our interest in phenomena induced by the NHSE, we will only consider OBCs in what follows.

As shown in Ref. [37], the BKC Hamiltonian $\hat{H}$ in Eq. (1) can be mapped to a bosonic particle-conserving tight-binding chain via local unitary squeezing (i.e., Bogoliubov) transformations. This effective local change of basis can be compactly written as $\hat{d}_j = e^{-i\phi j}\hat{U}_j\hat{a}_j\hat{U}_j^\dagger$, with the unitaries given by

$$\hat{U}_j = \begin{cases} \hat{S}_j(r(j - j_0))\hat{S}_j(ir_0), & g < \Delta, \\ \hat{S}_j(ir_0), & g > \Delta, \end{cases} \tag{4}$$

where $\hat{S}_j(\zeta) := e^{(1/2)(\zeta\hat{a}_j^{\dagger 2} - \text{H.c.})}$ denotes the standard squeezing transformation on the jth site and j_0 is an arbitrarily fixed "gauge" parameter.

The parameters are given by $r_0 = \frac{1}{2}\tanh^{-1}(g/\Delta)$, $r = \frac{1}{2}\log\left(w + \sqrt{\Delta^2 - g^2}\right)/\left(w - \sqrt{\Delta^2 - g^2}\right)$, and $\phi = \pi/2$ for the nonreciprocal case $g < \Delta$, and $r_0 = \frac{1}{2}\tanh^{-1}(\Delta/g)$ and $\phi = \arctan\left(w/\sqrt{g^2 - \Delta^2}\right)$ for the reciprocal phase $g > \Delta$. After performing this transformation, the system is mapped in both cases to a simple tight-binding Hamiltonian

$$\hat{H} = \sqrt{w^2 + g^2 - \Delta^2}\sum_{j=1}^{N-1}(\hat{d}_j^\dagger\hat{d}_{j+1} + \text{H.c.}). \tag{5}$$

The eigenmodes of $\hat{H}$ are standing waves, which we denote by $\hat{b}_n$ such that $\hat{H} = \sum_n \varepsilon_n\hat{b}_n^\dagger\hat{b}_n$ with $\varepsilon_n := -2\sqrt{w^2 + g^2 - \Delta^2}\cos[\pi n/(N + 1)]$.

A few important points are in order. First, note that as one increases g across the nonreciprocity transition (i.e., from below Δ to above Δ), there is no signature of a transition in the eigenvalue spectrum: the bandwidth of our system always increases monotonically with g. Hence, the nonreciprocity-to-reciprocity transition on which we focus *cannot* be simply diagnosed by looking at the spectrum of the OBC system. Second, we stress that for both $g > \Delta$ and $g < \Delta$, our system has propagating quasiparticles. In the nonreciprocal phase $g < \Delta$, it is useful to think of the position-dependent squeezing in Eq. (4) in terms of a localization length $\xi = a/r$, where a is the lattice spacing. However, the emergence of this effective localization length does not impede quasiparticle propagation (i.e., the group velocity remains finite). The localization length diverges when $w = \Delta$ and the OBC system is unstable for any $\Delta \geq w$. While this is an interesting regime in its own right, in this work we restrict our attention to the stable regime $\Delta < w$, as this is the only regime in which there is steady-state entanglement. The asymptotic time dependence of unstable quadratic bosonic systems is characterized in Ref. [49]: for long times, the BKC will exhibit unbounded logarithmic EE growth for $w = \Delta$ and will exhibit linear EE growth for $w > \Delta$. Finally, we note that to compute the EE of a subsystem of size A, one can work either with the $\hat{a}_j$ or the $\hat{d}_j$ operators, as they are related to one another by purely local transformations.

III. ENTANGLEMENT PHASE TRANSITION

We now turn to the study of the entanglement scaling across the different phases. In Ref. [29], it has been argued that nonreciprocity is detrimental for entanglement generation, as the quasiparticle pairs responsible for entanglement growth [50] propagate in the same direction, thus preventing the generation of long-range correlations and precluding any volume-law scaling of EE in the nonreciprocal phase. Here, we show that the BKC, while presenting the main features of a non-Hermitian nonreciprocal system (e.g., the NHSE and nonreciprocal transport) deviates dramatically from this expectation. While the reciprocal phase indeed presents a volume law as expected, we will show that the nonreciprocal phase, on the contrary, fulfills a *supervolume* law as defined in Sec. I.

We consider the following setup. We fix the initial state to be the physical vacuum (i.e., $\forall j, \hat{a}_j |\psi\rangle = 0$) and allow it to evolve under the BKC Hamiltonian for a long time. Since the system is dynamically stable, the time-averaged EE of a subsystem will eventually converge to some steady-state value. For Gaussian states, the covariance matrix σ fully determines the EE of any subsystem σ [49,51,52]. The EE of a subsystem A of size l is obtained from the relation

$$S_A = \sum_{n=1}^{l} s(\nu_n), \tag{6}$$

where

$$s(x) := \frac{x+1}{2} \ln \frac{x+1}{2} - \frac{x-1}{2} \ln \frac{x-1}{2} \tag{7}$$

and ν_n are the positive eigenvalues of $i\Omega\sigma|_A$, in which $|_A$ means that we truncate the support of the matrix to A. Our quantity of interest will be the long-time averaged quantity $\overline{S}_A$, where we use the overline to denote time-averaged quantities:

$$\overline{f(t)} \equiv \lim_{T\to\infty} \frac{1}{T} \int_0^T f(t) dt. \tag{8}$$

Before examining the EE, we look at the time-averaged position-dependent particle density across the chain. We observe that, as expected, the nonreciprocal phase has particles exponentially localized to the edges [Fig. 2(a)], while the reciprocal phase does not. Thus, one may expect that, in the reciprocal phase, taking a cut of the system from the left and increasing its size will not lead to a significant increase of the particle number and, consequently, no significant increase in the EE. However, this is not the case. To illustrate this fact, we plot in Fig. 2(b) the so-called Page curve [53], i.e., the EE of a subsystem of size l as a function of l while keeping the total system size N fixed. One finds that the reciprocal and nonreciprocal phases yield almost identically shaped curves. We conclude, perhaps surprisingly, that the BKC does not show any area-law phase induced by nonreciprocity.

To more fully understand the entanglement properties, we can also consider the scaling of subsystem EE in a slightly different manner. Instead of fixing the total system size N and varying the subsystem size, we can fix the subsystem size l to be a fraction of the total system size, $l = z \times N$, and then vary the total system size while keeping z fixed. For concreteness, we take $z = 1/4$ in what follows. The results for this scenario are presented in Fig. 3(a) for $w = 1$, $\Delta = 0.25$, and a range of g close to Δ. Usually, one does not have to worry about the total system size as long as it is large enough; however, here, we find drastically different phenomena. When scaling the total system size, we immediately observe the emergence of two phases—a "supervolume"-law phase, where the EE scales as N^2, corresponding to the nonreciprocal phase $g < \Delta$, and a volume-law phase, where the EE scales as N, corresponding to the reciprocal phase $g > \Delta$. The two are separated by a logarithmic scaling $N \log N$ when $g = \Delta$.

From these considerations and following the fitting procedure in, e.g., Ref. [2], we attempt the following

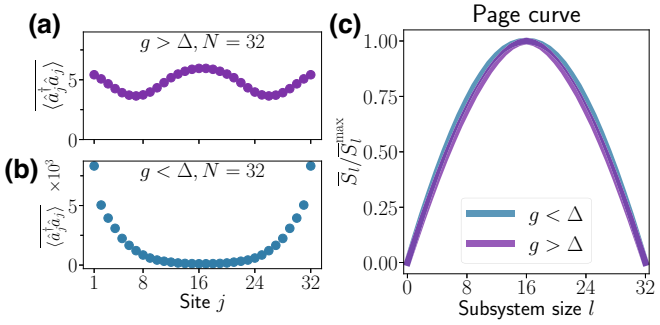

FIG. 2. A comparison of the average-density and Page curves for the reciprocal (with $g = 0.3$) and nonreciprocal (with $g = 0.24$) phases, for $w = 1, \Delta = 0.25, N = 32$. (a) The time-averaged position-dependent particle number $\langle \hat{a}_j^\dagger \hat{a}_j \rangle$, in the reciprocal phase. (b) The same as (a) but in the nonreciprocal phase. Note the difference in shape and the increase in scale in going from (a) to (b). (c) The EE for a cut of size l, with the subsystem being the left l sites of the chain in both the nonreciprocal and reciprocal phases. The curves are normalized by their maximum values. Despite the dramatic differences between (a) and (b), the Page curves are hardly distinguishable.

finite-size scaling for the EE,

$$\overline{S_{N/4}(g,\Delta,N)} - \overline{S_{N/4}(\Delta,\Delta,N)} = Nf\left((g^2-\Delta^2)N^{1/\nu}\right), \tag{9}$$

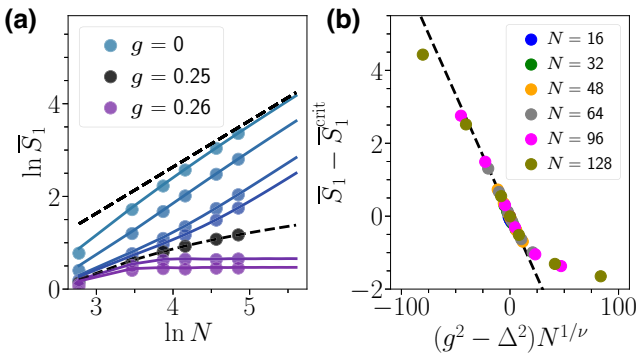

FIG. 3. (a) A log-log plot of the long-time-averaged EE for the EE of the leftmost site 1. The fixed parameters are $w = 1$ and $\Delta = 0.25$. The values of g for the lines from blue to purple are 0, 0.2, 0.24, 0.245, 0.25, 0.255, and 0.26. The scatter plots indicate values obtained from numerical simulation, whereas the solid lines are the analytical prediction from Eqs. (16) and (22). We observe good agreement between the two for all but the smallest chain size. The upper dashed line indicates the Nr scaling in the nonreciprocal phase and the lower dashed line indicates the single-site EE at the critical point $g = \Delta$ that separates the two phases. The two distinct scalings, with N in the nonreciprocal phase, and saturating in the reciprocal phase, are readily apparent. (b) The scaling collapse for the single-site EE with $\nu = 0.5$ in Eq. (24). The black dashed line is the expansion near the critical point obtained from the analytical form of the entropy [see Eqs. (18) and (23)].

and find that, fixing the critical exponent $\nu = 0.5$, it yields a good-quality collapse of the EE for different system sizes onto the same curve [see Fig. 3(b)].

We thus have established a key result of our work: despite the lack of measurements, postselection or disorder, our BKC model exhibits a clear entanglement phase transition as a function of g, one that coincides with the transition from a reciprocal to nonreciprocal phase.

IV. ANALYTICAL PROOF OF ENTANGLEMENT PHASE TRANSITION FOR A MINIMAL BIPARTITION

Computation of the postquench EE analytically, even for free systems, is in general a formidable task [54–56]. In this section, we provide analytical insight by studying the EE for the simpler *minimal-bipartition* case, i.e., the case where the subsystem A is composed of a single site. We will see that a transition from a phase where the EE is $O(N)$ to a phase where the EE is $O(1)$ already occurs for this case when increasing g above Δ.

For a single site j, the instantaneous symplectic eigenvalue ν_t at time t is given by

$$\nu_t^2 = \left(2\langle \hat{d}_j^\dagger \hat{d}_j \rangle_t + 1\right)^2 - 4|\langle \hat{d}_j \hat{d}_j \rangle_t|^2, \tag{10}$$

where we recall that $\hat{d}$ refers to the tight-binding basis defined in Eq. (4). The associated EE is simply $S_1 = s(\nu_t)$. For now, we have not specified a particular site. Given the strong spatial nonuniformity in the density in the nonreciprocal phase [see Fig. 2(b)], one would naturally expect that S_1 would depend strongly on the choice of site, with large values at the boundary and small values in the middle of the chain. Surprisingly, this is not the case. Equation (4) already highlights how this can be. It shows succinctly that the entanglement is not simply determined by the average photon number alone: one also needs to understand how many of these photons are associated with purely local-squeezing correlations and separate out this contribution. As we will see, despite the average density being highly inhomogeneous, S_1 is largely independent of the position j of the chosen site.

A. Nonreciprocal phase

In the nonreciprocal phase, we expect ν_t to be exponentially large with N, so that S_1 grows as N. When ν_t is large, the EE takes a simple form: to leading order in ν_t, $S_1 \approx \frac{1}{2} \ln \nu_t^2$. We will compute the time-average of the entropy, $\overline{S_1}$. In general, $\overline{\ln \nu_t^2} \neq \ln \overline{\nu_t^2}$ but it would be desirable to use the latter expression as it is much easier to compute. To quantify the error resulting from this approximation, we Taylor expand $\ln \nu_t^2$ with respect to ν_t^2 around

$\overline{\nu_t^2}$ and take the average, obtain

$$\overline{\ln \nu_t^2} = \ln \overline{\nu_t^2} + \frac{\overline{(\nu_t^2 - \overline{\nu_t^2})^2}}{2(\overline{\nu_t^2})^2} + \dots \tag{11}$$

We show in Appendix F that the second term is of order $O(1)$ because of cancellation of exponential-in-N contributions to the numerator and denominator. Hence,

$$\overline{S_1} \simeq \frac{1}{2} \ln \overline{\nu_t^2}. \tag{12}$$

Finally, to compute $\overline{\nu_t^2}$, we will make use of the fact that

$$\begin{aligned} &\overline{\langle \hat{d}_j^\dagger \hat{d}_j \rangle^2} - \overline{|\langle \hat{d}_j \hat{d}_j \rangle|^2} \\ &\quad = \left(\overline{\langle \hat{d}_j^\dagger \hat{d}_j \rangle}^2 - \left| \overline{\langle \hat{d}_j \hat{d}_j \rangle} \right|^2 \right) (1 + O(1/N)), \end{aligned} \tag{13}$$

a property that we prove in Appendix F. Remarkably, the neglect of fluctuations, implicit in this approximation, only holds for this difference and not for each term individually. More explicitly, one finds that $\overline{\langle \hat{d}_j^\dagger \hat{d}_j \rangle^2} \neq \overline{\langle \hat{d}_j^\dagger \hat{d}_j \rangle}^2$, and $\overline{|\langle \hat{d}_j \hat{d}_j \rangle|^2} \neq \left| \overline{\langle \hat{d}_j \hat{d}_j \rangle} \right|^2$. Our interpretation of this result is that while individual sites are subject to (exponentially) large temporal fluctuations in density, these fluctuations are almost entirely due to fluctuations in the amount of local pairing correlations. The contributions of these fluctuations (density, local pairing) thus cancel each other to leading order when calculating the symplectic eigenvalue and, consequently, the EE. Hence, to compute $\overline{\nu_t^2}$, one only needs the average covariance $\overline{\sigma}$. Taken together, all these steps considerably simplify the task of computing the EE and allow us to have quantitative results.

To compute $\overline{\sigma}$, we will consider the continuum limit, which we define as follows. Let a be the lattice spacing: we consider the limit $N \to \infty$, $a \to 0$, while keeping fixed the dimensionful quantities $\xi := a/r$ (the localization length), $L := a(N+1)$ (the system size), $x := aj$, and $p := \pi n / a(N+1)$. We are free to fix the parameter $x_0 = aj_0$. For the particular choice of $x_0 = L/2$, the correlations have a compact expression (see Appendix C):

$$\overline{\langle \hat{d}_x^\dagger \hat{d}_x \rangle} = \cosh(2r_0) \frac{\sinh(L/\xi)}{2L/\xi} - \frac{1}{2}, \tag{14}$$

$$\overline{\langle \hat{d}_x \hat{d}_x \rangle} = (-1)^{\frac{x}{a}} \frac{i}{2} \sinh(2r_0). \tag{15}$$

We see that the time-averaged local density and pairing correlations in the squeezed frame are *spatially uniform*. At first glance, this could seem surprising, as in this frame, our initial condition (vacuum in the laboratory frame) is extremely nonuniform in space, due to the position-dependent squeezing transformation in Eq. (4). However, the resulting uniformity of the time-averaged state can be understood by the dynamics being equivalent to a simple tight-binding chain. Indeed, for such a model, any spatial product state will lead to an average homogeneous profile in the continuum limit.

This in turn means that the EE in the minimal-bipartition protocol will yield the same result, independent of our choice of which site to single out. Heuristically, this explains the discrepancy between Figs. 2(b) and 2(c): while the average density in the laboratory frame is exponentially localized toward the edges, this excess density can largely be attributed to local squeezing, which does not affect the entanglement properties, in line with our interpretation of Eq. (13) (for further discussion about the separation between local squeezing and thermal occupation, see Appendix E). Inserting [Eqs. (14) and (15)] in Eq. (10) leads to

$$\overline{\nu_t^2} \approx 1 + \cosh^2(2r_0) \left(\frac{\sinh^2(L/\xi)}{(L/\xi)^2} - 1 \right). \tag{16}$$

Away from the critical point, the large-L limit gives us that

$$\overline{S_1} \approx L/\xi. \tag{17}$$

To obtain the scaling near the critical point, we consider the limit $L/\xi \ll 1$ for which the localization length ξ is far greater that the system size. This (see Appendix D) leads to:

$$\overline{S_1} \approx \ln N + \frac{1}{15} \frac{\Delta^2 - g^2}{w^2} N^2. \tag{18}$$

B. Reciprocal phase

In the reciprocal phase, the local correlations are given in the continuum limit by

$$\langle \hat{d}_x^\dagger \hat{d}_x \rangle = \frac{1}{2} (\cosh(2r_0) - 1), \tag{19}$$

$$\overline{\langle \hat{d}_x \hat{d}_x \rangle} = (-1)^{x/a} \frac{\sinh(2r_0)}{2} \frac{e^{i\varphi L} - 1}{\varphi L}, \tag{20}$$

where we have defined $\varphi := 1/a(\pi - 2\phi)$. We find that the average density in the squeezed frame is both time independent and spatially uniform. This is no surprise: in the reciprocal phase, the transformation to go to the squeezed frame [c.f. Eq. (4)] is uniform; hence our initial prequench state is also uniform. Such a density profile will not evolve under a tight-binding Hamiltonian. In contrast to this, the time-averaged local-squeezing correlators above retain a position dependence in their phase.

Away from the transition, i.e., for φ finite, the local pairing correlations tend to zero in the large-L limit. Thus the EE is simply

$$S_1 \approx s\left(\frac{g}{\sqrt{g^2-\Delta^2}}\right), \tag{21}$$

where $s(x)$ is defined in Eq. (7). Close to the transition, the eigenvalue scales like N and we can apply the same set of approximations as used in the reciprocal case. The eigenvalue corresponding to [Eqs. (19) and (20)] is

$$\overline{\nu_t^2} \approx 1+\sinh^2(2r_0)\left(\frac{2\,(1-\cos(\varphi L))}{(\varphi L)^2}-1\right). \tag{22}$$

Close to the critical point, the limit $\varphi L \ll 1$ leads to

$$\overline{S_1} \approx \ln N + \frac{1}{15}\frac{\Delta^2-g^2}{w^2}N^2, \tag{23}$$

which is consistent with the limit Eq. (18) from the nonreciprocal phase.

C. Numerical simulation and scaling collapse

Numerical simulations of the EE for a single site are plotted in Figs. 3(a) and 3(b) alongside analytical estimates. We observe that for large system size, the EE of the nonreciprocal phase always goes to the L/ξ scaling, whereas the EE for the reciprocal phase saturates. The expressions Eqs. [(18) and (23)] suggest the following scaling collapse:

$$\overline{S_1(g,\Delta,N)}-\overline{S_1(\Delta,\Delta,N)} = f\left((g^2-\Delta^2)N^{1/\nu}\right), \tag{24}$$

with $\nu = 0.5$, thus proving Eq. (9) for the minimal bipartition. Note that not only the power laws are in agreement with the numerics but also the nonuniversal $1/15$ prefactor of the second term of Eqs. [(18) and (23)] (see Fig. 3).

Before leaving this section, we wish to highlight a crucial fact: entanglement in our system *cannot* simply be predicted from the behavior of the average photon number. A naive argument would be that the average photon number on each site of the postquench state determines its effective Hilbert-space dimension D_j, which would then (assuming thermalization) set its entropy. This line of reasoning would suggest that the entropy of a given site should correspond to the entropy of a single bosonic mode in a thermal state, i.e.,

$$\bar{S}^{(j)}_{1,\mathrm{th}} = s\left(\overline{\langle \hat{a}_j^\dagger \hat{a}_j\rangle}\right) \sim \log \overline{\langle \hat{a}_j^\dagger \hat{a}_j\rangle} \sim \log D_j, \tag{25}$$

where the first approximation holds for large particle numbers. If this reasoning were true, then in the nonreciprocal phase, the entropy-versus-position curve should be peaked at the edges, reflecting the skin-effect-induced localization of the particle-number density. As shown explicitly in Fig. 4, this prediction is manifestly incorrect. The numerics here match the analytical arguments presented above: the true single-site entropy is almost independent of position and shows no signature of localization. As such, simply understanding how the average particle number depends on the system parameters does not immediately let one understand the entanglement properties. The discrepancy between the particle number and the EE is further explored in Appendix E.

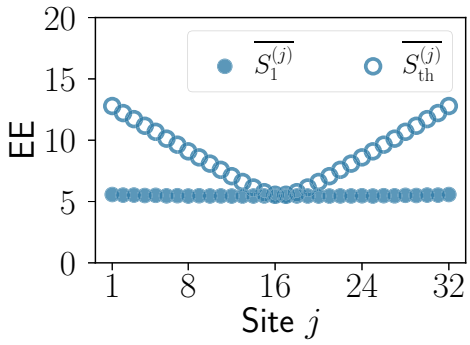

FIG. 4. The filled circles show the one-site EE $\overline{S_1^{(j)}}$ as a function of position j in the nonreciprocal phase, for parameters $N = 32$, $w = 1$, $g = 0$, and $\Delta = 0.25$. Despite being in the skin-effect phase, the entropy is almost completely uniform. The open circles show $\overline{S_{\mathrm{th}}^{(j)}}$, the prediction for the single-site entropy based using the average photon number alone, cf. Eq. (25). This prediction deviates sharply from the true result. This highlights an important caveat: simply using the average particle number as a proxy for entanglement can be extremely misleading.

V. GENERALIZED GIBBS ENSEMBLE

In this last section, we show how the previous results can be extended to understand the EE of small subsystems for size l satisfying $l/N \ll 1$. To do this, we make a local-thermalization hypothesis that the subsystem will be described by a generalized Gibbs ensemble (GGE) state [57,58]. The GGE ansatz amounts to the assumption that the expectation value of the local observables can be extracted from

$$\hat{\rho}_{\mathrm{GGE}} := \frac{1}{Z}e^{\sum_n \beta_n \hat{b}_n^\dagger \hat{b}_n + \gamma_n \hat{b}_{\bar{n}}^\dagger \hat{b}_n^\dagger + \gamma_n^* \hat{b}_n \hat{b}_{\bar{n}}}, \tag{26}$$

where we recall that the $\hat{b}_n$ modes refer to the standing-wave basis, Z is a normalization factor, $\{\beta_n, \gamma_n, \gamma_n^*\}$ are thermodynamic variables fixed by the initial condition, and $\bar{n}$ is defined by the relation $\varepsilon_{\bar{n}} = -\varepsilon_n$. Note the contribution of the pairing terms $\hat{b}_{\bar{n}}^\dagger \hat{b}_n^\dagger$ and $\hat{b}_n \hat{b}_{\bar{n}}$ that do not appear in $\hat{H}$. For free bosonic system, this is simply the time average of $\hat{\rho}$: $\hat{\rho}_{\mathrm{GGE}} = \overline{\hat{\rho}}$.

In a similar fashion, the GGE ansatz for entanglement is that the EE of a subsystem A can be extracted from $\hat{\rho}_{\mathrm{GGE}}$ [59], i.e., that one has

$$S_A^{\mathrm{GGE}} = \frac{l}{N}\sum_{n=1}^{N} s(\nu_{\mathrm{GGE}}^n), \tag{27}$$

where ν_{GGE}^n are the positive eigenvalues associated with $\sigma_{\mathrm{GGE}}\Omega$. Given the breaking of translational invariance in the steady state, as exemplified by the strong inhomogeneity in the local occupation number as seen in Fig. 2(b), and the fact that the GGE is agnostic about the cut chosen for A, one may expect this approach to fail. On the other hand, the fact that the local correlations are spatially uniform in the tight-binding frame suggests that, for the purpose of computing the EE, the GGE might be enough.

In the nonreciprocal phase, fixing our gauge parameter to $x_0 = 0$, the positive eigenvalue of Eq. (D2) in the continuous limit is (for the derivation, see Appendix D)

$$\nu_p = \sqrt{\cosh^2(2r_0)\left(\left(\frac{(p\xi)^2}{1+(p\xi)^2}\frac{\sinh(L/\xi)}{L/\xi}\right)^2 - 1\right) + 1}. \tag{28}$$

We see that the localization length ξ is the natural scale separating the long- and short-wavelength physics. The suppression of ν_p for $p\xi \ll 1$ is a direct consequence of low-momentum standing waves having small wavefunction amplitudes near the system boundary.

In the localized regime $\xi \to 0$, the dominant contribution in the above expression is $\sinh^2(L/\xi)$. Since the entanglement is proportional to the log, we have

$$s(\nu_p) \approx \log \nu_p \approx L/\xi. \tag{29}$$

We see that, because of the exponential scaling of the ν_p with L, the contributions of the different modes to the entanglement become *independent* of p.

Remarkably, a similar statement is true close to the transition, where $\xi \to \infty$. In this regime, the momentum dependence in Eq. (28) cancels out and we are left with

$$\nu_p \approx \cosh(2r_0)\sqrt{\left(\frac{\sinh(L/\xi)}{L/\xi}\right)^2 - 1}, \tag{30}$$

which is again independent of p.

Similarly, in the reciprocal phase, we have

$$\nu_p = \sqrt{1+\sinh^2(2r_0)\left(1 - \frac{32p^4\,(1-\cos(\varphi L))}{\left(\varphi L\left(4p^2-\varphi^2\right)\right)^2}\right)}, \tag{31}$$

where we have defined $\varphi := 1/a(\pi - 2\phi)$. For finite φ, this quantity becomes p independent in the large-L limit. Close to the critical point, $\varphi \to 0$, keeping φL finite, while $L \to \infty$ gives

$$\nu_p \approx \sqrt{1+\sinh^2(2r_0)\left(1 - \frac{2\,(1-\cos(\varphi L))}{(\varphi L)^2}\right)}, \tag{32}$$

which is also p independent. Thus, we see that in all regimes of interest, for the purpose of computing entanglement, the momentum dependence drops out. This in turn implies that the GGE and the minimal bipartition will match in all the limits mentioned above and thus

$$S_A^{\mathrm{GGE}} = l\overline{S_1}. \tag{33}$$

Interestingly, this means that for computing the EE, the local-thermalization assumption yields accurate results, despite the fact the system is both strongly inhomogeneous and subject to exponentially large fluctuations. Our interpretation is that fluctuations in local quantities mainly come from a variation in the squeezing strength, which leaves the EE property unchanged.

VI. CONCLUSIONS

Our work demonstrates the existence of an entanglement phase transition in a nondisordered bosonic system undergoing purely unitary evolution. When varying the hopping parameter g below a critical value Δ, the system undergoes a transition from a reciprocal to a nonreciprocal phase, accompanied by a transition from a volume law to a *supervolume* law for the postquench EE of a subsystem. While our system shares many common features with non-Hermitian systems, it *does not* involve measurement or postselection in any way. Our study suggests that the breaking of reciprocity can be associated with entanglement transitions even in settings where there is no competition between unitary dynamics and measurement-induced nonunitary evolution.

It is interesting to contrast our results with the related non-Hermitian fermionic model studied in Ref. [29], involving two coupled Hatano-Nelson chains. As discussed, that model exhibits identical spectral properties and NHSE as our system. In Ref. [29], an entanglement transition has also been found coinciding with the breaking of reciprocity but, unlike us, the authors have found that the entanglement generation is greatly suppressed in the nonreciprocal phase (yielding only area-law behavior). In contrast, our nonreciprocal phase exhibits marked directional transport but no area-law entanglement behavior (and, in fact, enhances the entanglement scaling). This suggests that the unidirectional quasiparticle picture proposed in Ref. [29] is not applicable to generic entanglement transitions associated with reciprocity breaking.

The stark differences between our results and those in the model studied in Ref. [29] can be attributed to particle

statistics. Our model is bosonic, whereas that in Ref. [29] is fermionic. In our case, we show that nonreciprocity largely manifests itself in the steady state as large amounts of local-squeezing correlations (e.g., on-site pairing). Such squeezing does not affect the entanglement properties and has no analogue in fermionic systems. Another intuitive, albeit crude, way to understand this difference is to note that directional transport for fermions necessarily results in a highly pure states for sites near the edges: once a site fills up, it decouples from the rest of the system. Conversely, there is no analogous mechanism by which transporting bosons to sites on the edge could decouple them. Both of these phenomena are due to the unbounded local Hilbert space of a bosonic system. Finally, the supervolume law that we identify is unique to bosonic systems, as it is simply impossible for the entanglement of fermionic systems to grow superextensively, or any faster than the size of the associated Hilbert space.

It is also interesting to note that in contrast to other studies of bosonic systems, we observe the existence of an EPT despite the absence of measurements [45,60] and nonlinearities (see, e.g., Ref. [61]). We also mention that for fermionic systems, entanglement transitions have been observed for free unitary disordered systems; these have been directly tied to either Anderson or many-body localization-delocalization transitions (see, e.g., Refs. [62–64]). These disorder-driven EPTs are also distinct from the phenomenon that we describe, as (apart from boundaries) our system is fully translationally invariant.

While our focus in this work has been on postquench EE, it is important to note that the reciprocity-breaking transition in our model can also be characterized with other quantities. This comprises the spectrally heralded reciprocal-to-nonreciprocal transition already pointed out in Ref. [37]. Another observable that shows clear signatures of the transition is the scaling of the total particle number with N in the postquench state, a quantity that is *linear* in ρ. Such signatures of the transition differ markedly from the phenomenology of standard MiPT, where the transition can *a priori* only be characterized using quantities nonlinear in ρ. We stress that the phase transition in the non-Hermitian model of Ref. [29] could also be characterized using a single observable, the total current. Returning to our model, we stress that even though the reciprocal and nonreciprocal phases differ strongly in terms of their average density, this does not by itself let one infer the existence of an EPT. In general, the particle number can be made arbitrarily large by means of local-squeezing transformations, something that would have no impact on entanglement. The fact that the average density and the entanglement properties can be extremely different is demonstrated explicitly in Fig. 4 and Appendix E, where we observe that the EE spatial structure is dramatically different from that of the average particle number.

The EPT demonstrated in this work is experimentally appealing for several reasons. First, since the model is a nondisordered closed system, postselection is a complete nonissue. Second, all the studied dynamics are Gaussian, which for bosonic systems are generally considered much more experimentally tractable. Finally, as we have shown in Sec. IV, the entire EPT can be characterized by a single-site covariance matrix. Hence, to detect and characterize the EPT experimentally, one only needs to characterize the correlations of a single site.

In this work, we have demonstrated and characterized an EPT associated with a transition from nonreciprocity to reciprocity in a particular model, namely, the BKC. Future work could investigate the more general relationship between nonreciprocity and entanglement—in particular, how many of the features of this EPT generalize to other models and what one can say more generally about the entanglement properties of nonreciprocal models. Finally, we note that while entanglement is a quantum property, one could also investigate a classical version of this model and ask whether the nonreciprocal-to-reciprocal transition there is also heralded by a transition in correlation measures besides entanglement.

ACKNOWLEDGMENTS

We thank Vincenzo Alba and Gilles Parez for useful discussions. This work was supported by the Air Force Office of Scientific Research under Grant No. FA9550-19-1-0362. A.C. also acknowledges support from the Simons Foundation through a Simons Investigator Award (Grant No. 669487, A.C.).

APPENDIX A: DETAILS ON THE NUMERICS

We are interested in the long-time-averaged entanglement that results from the quench dynamics described in the main text, and hence the quantity of interest is

$$\overline{S_t} = \lim_{T\to\infty} \frac{1}{T}\int_0^T S_t dt, \tag{A1}$$

which is the EE for some subsystem of our 1D BKC lattice for some fixed set of parameters. Without loss of generality, we will fix $w = 1$ and $\Delta = 0.25$, and vary g, N, where Δ and g will be written in units of w. We will estimate $\overline{S_t}$ by numerically calculating S_t for some discrete set of times and then taking the mean. Since we want the EE in the quasisteady state, we only need to perform this calculation up to some finite large T for which the estimate of $\overline{S_t}$ converges to some desired accuracy. Since the evolution of S_t is deterministic, we can set the accuracy to any level we want.

In general, one might not expect to be able to simulate arbitrarily large times accurately for nonreciprocal systems, due to the issue of numerical ill conditioning. Fortunately, we can avoid this by performing the simulations in the squeezing frame defined by Eq. (4), something that is possible whenever $g \neq \Delta$. For $g = \Delta$, the squeezing frame

is not well defined. In that case, we have simply performed the simulations in the laboratory frame and found it to be stable for all chosen parameters in this work.

The following are additional important points about the numerical approach used to calculate the EE:

(1) The values of the EE at initial small times t are in general not representative of the quasisteady state of interest. While they get averaged away at long times, including these points slows down the convergence of our calculation. We thus pick an initial time $T_{\min}$ at which S_t has approximately relaxed to its quasisteady-state value and only use $t \geq T_{\min}$ to calculate the needed average. In the tight-binding frame, we can read off the group velocity as J and hence we expect the system to relax with time scale $O(N/J)$. For convenience, we pick $T_{\min} = 10N/J$, where 10 is a reasonably large prefactor.

(2) Next, we pick an initial set of times $\{T_1, \ldots, T_{1000}\}$. We do so by picking a uniformly spaced set of times with $T_1 = T_{\min}, T_{k+1} - T_k = \delta T$. To aid convergence, we want δT to be relatively large compared to the time scale of oscillations in the quasisteady state, which we generally expect to occur on the time scale $O(1/J)$. Again, we pick 10 as an arbitrary reasonably large prefactor and set $\delta T = 10/J$.

(3) We numerically calculate the values $\{S_{T_1}, \ldots, S_{T_{1000}}\}$ and estimate $\widetilde{\overline{S}}_t = \frac{1}{1000}\sum_i S_{t_i}$. We use $\widetilde{\varepsilon} = s/\sqrt{N}$, where s is the standard deviation of the set $\{S_{T_1}, \ldots, S_{T_{1000}}\}$, to estimate the accuracy of $\widetilde{\overline{S}}_t$.

(4) We want the relative error (compared to the mean) to be small, so we pick an arbitrary harsh convergence criterion $\widetilde{\varepsilon}/\widetilde{\overline{S}}_t < 0.001$. If this is satisfied, we are done. Otherwise, we repeat the procedure for another 500 time steps $\{T_{1001}, \ldots, T_{1500}\}$ selected in the same way and check the convergence criterion, repeating until it is satisfied.

Finally, we have numerically verified that this simulation is insensitive to the exact values of each of the prefactors stated above. For the convergence threshold $\widetilde{\varepsilon}/\widetilde{\overline{S}}_t < 0.001$ that we have picked, the error bars are not visible on the plots and we have chosen to omit them. The simulations in Figs. 1 and 3 are performed for $g = 0$, 0.2, 0.24, 0.245, 0.249, 0.25, 0.251, 0.255, and 0.26 and $N = 16$, 32, 48, 64, 96, and 128.

APPENDIX B: FULL TIME EVOLUTION AND FLUCTUATIONS OF EE IN THE NONRECIPROCAL PHASE

In this appendix, we numerically study the fluctuations in the EE in the quasisteady state of the nonreciprocal phase, in order to demonstrate that the mean EE is a meaningful characterization of the quasisteady state. In other words, fluctuations in the EE over time in the long-time regime are sufficiently small or comparable to the mean value. Surprisingly, this is true even though it is not the case for any of the other quantities of interest, such as ν_t, ν_t^2, $\overline{\langle \hat{d}^\dagger \hat{d} \rangle}$, where fluctuations can be significantly larger than the mean value.

We expect fluctuations to be largest when the nonreciprocity is maximum. In terms of the numerics provided in the main text, this is when $g = 0, \Delta = 0.25, w = 1$. Figures 5(a) and 5(c) plot the full time evolution of the EE for $N = 16$, 32, 48, and 64 for the $N/4$ bipartition and the minimal bipartition. We observe, at least visually, that the EE does indeed reach a quasisteady state, with fluctuations over time much smaller than the average value.

We can quantify the size of the fluctuations compared to the mean value using the quantity

$$\frac{\sqrt{\overline{(S_t - \overline{S}_t)^2}}}{\overline{S}_t}, \tag{B1}$$

where we calculate the time-averaged quantities using the methods outlined in Appendix A. These quantities are plotted in Figs. 5(b) and 5(d) for values of N up to $N = 64$ and $g = 0$, 0.2, 0.24, 0.245, and 0.249 and observe that the above quantity generally decreases with N, giving a value of approximately 10^{-2}–10^{-1} across all N considered. We comment that this property does not hold for other quantities, such as ν_t or the particle density. Furthermore, note that we do not require this quantity to go to zero—simply that it is reasonably small enough that the time-averaged EE provides a good description of the quasisteady state.

We comment briefly on the time dependence of the EE (prior to saturation) in the supervolume-law phase. In the volume-law phase, the EE simply grows linearly before saturating and oscillating around its steady-state value—this behavior is well understood in the quasiparticle picture, where one assumes that the system starts out with pairs of entangled quasiparticles the ballistic propagation of which explains the entanglement growth up to saturation [50].

Conversely, the time dependence of the EE in the supervolume-law phase at short and intermediate times displays features that are not immediately explained by the traditional quasiparticle ansatz. We focus on the case of the $l = N/4$ bipartition when $w = 1$, $\Delta = 0.25$, and $g = 0$, although the same features appear across all parameter values in the nonreciprocal phase. The short- and intermediate-time growth is shown in Fig. 6. At short times, the EE growth is in fact greater than linear, with a dependence that is independent of the system size N but depends on the parameters w, g, and Δ. For the parameters in Fig. 6, our numerics show that the EE grows as

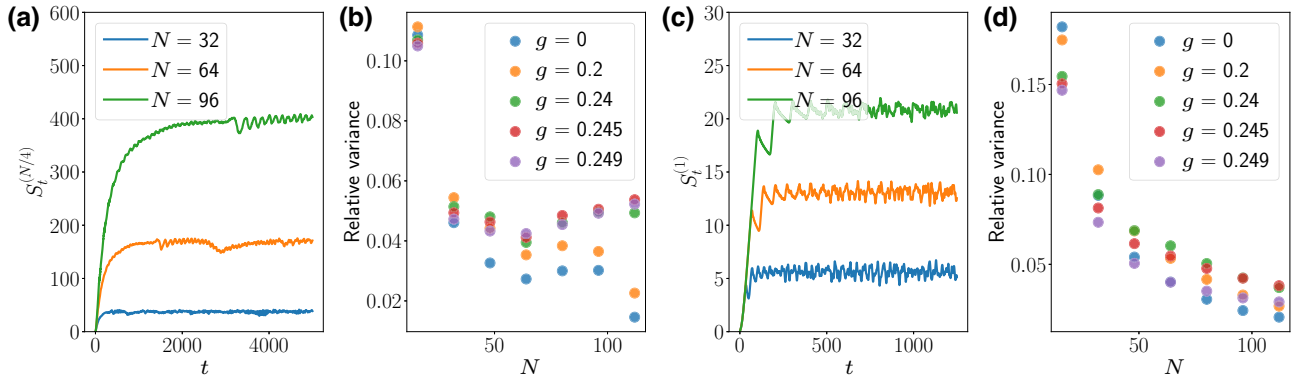

FIG. 5. (a) The full time evolution of the EE of the $(N/4 : 3N/4)$ bipartition for a representative time period for $w = 1$, $\Delta = 0.25$, and $= 0$. We observe that visually, the long-time EE appears to oscillate around some mean value, with oscillations that are small compared to the mean value. (b) The plot of the variance defined in Eq. (B1), calculated over the period of time required for the mean value of the EE to converge according to the criterion outlined in Appendix A. (c) The same as (a) but for the minimal bipartition $(1 : N - 1)$. (d) The same as (b) but for the minimal bipartition $(1|N - 1)$.

approximately $t^{1.69}$ for short times. At intermediate times, the temporal growth of EE starts to depend on the system size and saturate (the branching between the different curves in Fig. 6). Immediately after this branching, we find that the EE starts to display concomitant oscillations. This feature is also not present in predictions derived from a quasiparticle ansatz. These features merit further study, as they suggest that the quasiparticle ansatz needs to be significantly modified to account for squeezing in bosonic systems; we leave this to future work.

APPENDIX C: AVERAGE CORRELATIONS

In this appendix, we derive explicitly the time-averaged covariance $\overline{\sigma}$ both in the reciprocal and nonreciprocal phases. In particular, we will show that in the squeezed frame, $\overline{\sigma}$ is *independent* of the position in the lattice.

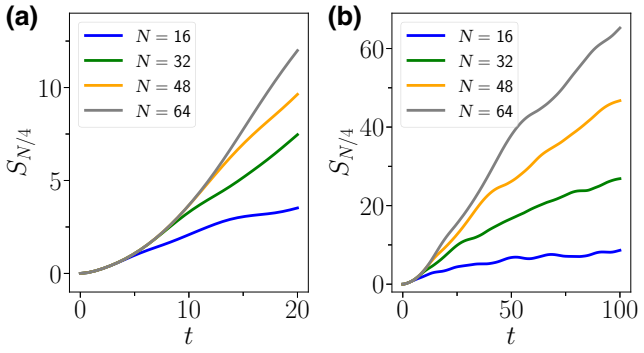

FIG. 6. The plot of the time evolution of the $S_{N/4}$, i.e., the EE of the $(N/4 : 3N/4)$ bipartition, for $w = 1$, $\Delta = 0.25$, $g = 0$, and $N = 16$, 32, 48, and 64. (a) The short-time evolution. We observe that the short-time evolution is independent of the system size and strictly superlinear. (b) The intermediate-time evolution. At intermediate times, the EE growth slows down before eventually saturating. Immediately after branching out from the short-time system-independent curve, the EE evolution starts to show concomitant oscillations.

In both the reciprocal and nonreciprocal phases, the Hamiltonian can be brought under the diagonal form $\hat{H} = \sum_n \varepsilon_n \hat{b}_n^\dagger \hat{b}_n$ with $\varepsilon_n = -2\sqrt{w^2 + g^2 - \Delta^2}\cos[\pi n/(N+1)]$.

The time average for the correlations in the position basis is particularly simple and can be written as the selection rules

$$\overline{\langle \hat{b}_m^\dagger \hat{b}_n \rangle} = \delta_{m,n} \langle \hat{b}_n^\dagger \hat{b}_n \rangle_{t=0}, \tag{C1}$$

$$\overline{\langle \hat{b}_m \hat{b}_n \rangle} = \delta_{m,\bar{n}} \langle \hat{b}_{\bar{n}} \hat{b}_n \rangle_{t=0}, \tag{C2}$$

where we have introduced $\bar{n} := N + 1 - n$. Hence the average state of the system is entirely determined by the values of these correlations at $t = 0$.

1. Nonreciprocal phase

In the nonreciprocal phase, the eigenmodes are given by

$$\begin{aligned}\hat{b}_n = \sqrt{\frac{2}{N+1}} \sum_{j=1}^{N} e^{-i\frac{\pi j}{2}} \sin\left(\frac{\pi j n}{N+1}\right) \Big(&(\cosh(r(j - j_0)) \\ &\times \cosh r_0 + i \sinh(r(j - j_0)) \sinh r_0)\, \hat{a}_j \\ &+ (i \cosh(r(j - j_0)) \sinh r_0 \\ &- \sinh(r(j - j_0)) \cosh r_0)\, \hat{a}_j^\dagger \Big), \end{aligned} \tag{C3}$$

where j_0 is an arbitrary "gauge factor," $\tanh(2r_0) = g/\Delta$, and $e^{2r} = (w + \sqrt{\Delta^2 - g^2})/(w - \sqrt{\Delta^2 - g^2})$. The

conserved correlations are fixed by the vacuum initial state

$$\langle \hat{b}_n^\dagger \hat{b}_n \rangle_{t=0} = v(n,r)\cosh(2r_0) - \frac{1}{2}, \tag{C4}$$

$$\langle \hat{b}_{\bar{n}} \hat{b}_n \rangle_{t=0} = w(n,r)\cosh(2r_0) - \frac{i}{2}\sinh(2r_0), \tag{C5}$$

with

$$v(n,r) := \frac{1}{N+1}\sum_j \cosh\left(2r(j-j_0)\right)\sin^2\left(\frac{\pi nj}{N+1}\right), \tag{C6}$$

$$w(n,r) := \frac{1}{N+1}\sum_j \sinh\left(2r(j-j_0)\right)\sin^2\left(\frac{\pi nj}{N+1}\right). \tag{C7}$$

These expressions simplify in the continuous limit defined as follows. Let a be the lattice spacing. We consider the limit $N \to \infty$, $a \to 0$, while keeping fixed the dimensionful quantities $\xi := a/r$, $L := a(N+1)$, $x := aj$, and $p := \pi n/a(N+1)$. To simplify the expressions, we fix the gauge parameter $j_0 = 0$. This leads to

$$v(p,\zeta) = \frac{\xi p^2}{2L\left(\xi^{-2}+p^2\right)}\frac{\sinh(2L/\xi)}{2}, \tag{C8}$$

$$w(p,\zeta) = \frac{\xi p^2}{2L\left(\xi^{-2}+p^2\right)}\frac{\cosh\left(2L/\xi\right)-1}{2}. \tag{C9}$$

a. Local correlations in the tight-binding basis

In this subsection, we derive the average local on-site correlations in a given spatial frame. As discussed in the main text, those are the quantities necessary to characterize entanglement in the minimal-bipartition protocol. The spatial frame where the correlations appear in their simplest form is the tight-binding frame with operators $\{\hat{d}_j^\dagger, \hat{d}_j\}$. The correlations are related to the one in the diagonal basis by a simple OBC Fourier transform:

$$\overline{\langle \hat{d}_j^\dagger \hat{d}_j \rangle} = \frac{2}{N+1}\sum_{n=1}^{N}\sin^2\left(\frac{\pi nj}{N+1}\right)\overline{\langle \hat{b}_n^\dagger \hat{b}_n \rangle}, \tag{C10}$$

$$\overline{\langle \hat{d}_j \hat{d}_j \rangle} = \frac{2}{N+1}(-1)^{j+1}\sum_{n=1}^{N}\sin^2\left(\frac{\pi nj}{N+1}\right)\overline{\langle \hat{b}_{\bar{n}} \hat{b}_n \rangle}. \tag{C11}$$

We will make use of the identity

$$\frac{2}{N+1}\sum_{n=1}^{L}\sin^2\left(\frac{\pi nj}{N+1}\right)\sin^2\left(\frac{\pi nl}{N+1}\right) \tag{C12}$$

$$= \frac{1}{2} + \frac{1}{4}\left(\delta_{j,l} + \delta_{j,N+1-l}\right). \tag{C13}$$

Inserting this identity in the previous relations leads to

$$\overline{\langle \hat{d}_j^\dagger \hat{d}_j \rangle} = -\frac{1}{2} + \frac{1}{N+1}\frac{\cosh(2r_0)}{2}\left(\frac{\sinh(rN)\cosh(r(N+1-2j_0))}{\sinh(r)} + \frac{1}{2}\left(\cosh\left(2r(j-j_0)\right) + \cosh\left(2r(N+1-j-j_0)\right)\right)\right), \tag{C14}$$

where we recall that j_0 is an arbitrary "gauge factor". Once again, this expression simplifies in the continuous limit:

$$\overline{\langle \hat{d}_x^\dagger \hat{d}_x \rangle} = \cosh(2r_0)\frac{\sinh(2(L-x_0)/\xi) + \sinh(2x_0/\xi)}{4L/\xi} - \frac{1}{2}. \tag{C15}$$

Note that the j-dependent term is no longer here in the continuous-limit description. Finally, we can fix the gauge parameter $x_0 = L/2$ to simplify these expressions:

$$\overline{\langle \hat{d}_x^\dagger \hat{d}_x \rangle} = \cosh(2r_0)\frac{\sinh(L/\xi)}{2L/\xi} - \frac{1}{2}. \tag{C16}$$

For the local pair-annihilation correlation, one obtains

$$\overline{\langle \hat{d}_j \hat{d}_j \rangle} = \frac{(-1)^{j+1}}{2}\left(-i\sinh(2r_0)\frac{1}{N+1}\cosh(2r_0)\left(\frac{\sinh(rN)\sinh(r(N+1-2j_0))}{\sinh(r)} + \frac{1}{2}\left(\sinh\left(2r(j-j_0)\right) + \sinh\left(2r(N+1-j-j_0)\right)\right)\right)\right). \tag{C17}$$

Once again, taking the continuous limit and choosing $x_0 = L/2$, one obtains

$$\overline{\langle \hat{d}_x \hat{d}_x \rangle} = (-1)^{\frac{x}{a}} \frac{i}{2} \sinh(2r_0). \tag{C18}$$

We thus see that in the continuous limit defined above, the norms of both correlations are independent of x in the tight-binding frame. For the minimal bipartition, this means that the value of the EE will be the same, up to finite-size corrections, for all the sites.

2. Reciprocal phase

In the reciprocal phase, the eigenoperators are

$$\hat{b}_n = \sqrt{\frac{2}{N+1}} \sum_j \sin\left(\frac{\pi n j}{N+1}\right) e^{-i\phi j} \times \left(\cosh r_0 \hat{a}_j + i \sinh r_0 \hat{a}_j^\dagger\right), \tag{C19}$$

where $\tanh(2r_0) = g/\Delta$ and $\phi = \arctan(w/\sqrt{g^2 - \Delta^2})$. The conserved correlations in this case are given by

$$\langle \hat{b}_n^\dagger \hat{b}_n \rangle_{t=0} = \overline{\langle \hat{b}_n^\dagger \hat{b}_n \rangle} = \frac{1}{2}(\cosh(2r_0) - 1), \tag{C20}$$

$$\langle \hat{b}_{\bar{n}} \hat{b}_n \rangle_{t=0} = \overline{\langle \hat{b}_{\bar{n}} \hat{b}_n \rangle} = -i \frac{\sinh(2r_0)}{2} \frac{2}{N+1} \times \sum_{j=1}^{N} \sin^2\left(\frac{\pi n j}{N+1}\right) e^{-2i(\phi - \frac{\pi}{2})j}. \tag{C21}$$

Performing the sum for $\overline{\langle \hat{b}_{\bar{n}} \hat{b}_n \rangle}$ in the continuous limit leads to

$$\overline{\langle \hat{b}_{\bar{p}} \hat{b}_p \rangle} = \frac{1}{L} \sinh(2r_0) \frac{2p^2 \left(1 - e^{i\varphi L}\right)}{\varphi\left(4p^2 - \varphi^2\right)}, \tag{C22}$$

where we have defined $\bar{p} := \pi/a - p$ and $\varphi := 1/a(\pi - 2\phi)$.

a. Local correlations in the tight-binding basis

As for the nonreciprocal case, the local on-site correlations take their simplest form in the tight-binding frame with operators $\{\hat{d}_j^\dagger, \hat{d}_j\}$. Performing the inverse Fourier transform leads in this case to

$$\overline{\langle \hat{d}_j^\dagger \hat{d}_j \rangle} = \frac{1}{2}(\cosh(2r_0) - 1), \tag{C23}$$

$$\overline{\langle \hat{d}_j \hat{d}_j \rangle} = i \frac{(-1)^j \sinh(2r_0)}{2(N+1)} \left(\frac{e^{i\theta j} + e^{i\theta(N+1-j)}}{2} - \frac{1 - e^{i\theta N}}{1 - e^{-i\theta}}\right). \tag{C24}$$

Defining $\varphi := \theta/a$, the last expression simplifies once again in the continuous limit:

$$\overline{\langle \hat{d}_x \hat{d}_x \rangle} = (-1)^{x/a} \frac{\sinh(2r_0)}{2} \frac{e^{i\varphi L} - 1}{\varphi L}. \tag{C25}$$

APPENDIX D: COMPUTATION OF ENTANGLEMENT ENTROPY

In this appendix, we compute the EE of a subsystem of size l in the limit $l/L \ll 1$ using the GGE. We begin by showing that, for our model, this is equivalent to the minimal-bipartition approach, both in the reciprocal and nonreciprocal phase.

1. Equivalence between GGE ansatz and minimal bipartition

Recall that in the GGE approach, the stationary entanglement of a subsystem A of size l is simply assumed to be directly proportional to the total EE of the total system, with the proportionality coefficient fixed by l,

$$S_A = \frac{l}{N} \sum_n s(\nu_n), \tag{D1}$$

where $s(x) := [(x+1)/2] \ln[(x+1)/2] - [(x-1)/2] \ln[(x-1)/2]$ and ν_n the positive eigenvalue associated with the 2×2 block matrix

$$\begin{pmatrix} 2\overline{\langle \hat{b}_n^\dagger \hat{b}_n \rangle} + 1 & -2\overline{\langle \hat{b}_{\bar{n}} \hat{b}_n \rangle} \\ 2\overline{\langle \hat{b}_{\bar{n}} \hat{b}_n \rangle}^* & -2\overline{\langle \hat{b}_n^\dagger \hat{b}_n \rangle} - 1 \end{pmatrix}. \tag{D2}$$

a. Nonreciprocal phase

Recall the expressions for the correlations in the continuous limit (recall that we fixed $x_0 = 0$ in this case):

$$\overline{\langle \hat{b}_p^\dagger \hat{b}_p \rangle} = \frac{(p\xi)^2}{2\left(1 + (p\xi)^2\right)} \frac{\sinh(2L/\xi)}{2L/\xi} \cosh(2r_0) - \frac{1}{2}, \tag{D3}$$

$$\overline{\langle \hat{b}_{\bar{p}} \hat{b}_p \rangle} = \frac{(p\xi)^2}{1 + (p\xi)^2} \frac{\sinh^2(L/\xi)}{2L/\xi} \cosh(2r_0) - \frac{i}{2} \sinh(2r_0) \tag{D4}$$

where $\pi/L \le p \le \pi/a$. The positive eigenvalue of Eq. (D2) is

$$\nu_p = \sqrt{\cosh^2(2r_0)\left(\left(\frac{\xi p^2}{L\left(\xi^{-2} + p^2\right)}\right)^2 \sinh^2(L/\xi) - 1\right) + 1}. \tag{D5}$$

Away from the critical point, ζ is finite. Taking the large-system-size limit then leads to

$$\nu_p \approx \frac{\xi p^2}{L\left(\xi^{-2}+p^2\right)} \cosh(2r_0)\sinh(L/\xi). \tag{D6}$$

Importantly,

$$s(\nu_p) \approx \ln \nu_p \approx L/\xi, \tag{D7}$$

to leading order. Thus we see that to leading order in L, the momentum dependence of the mode is irrelevant and all modes give the same contribution.

Close to the transition, $\xi \to \infty$, $r_0 \to \infty$. Taking the limit $L \to \infty$ while keeping L/ξ finite leads to

$$\nu_p \approx \cosh(2r_0)\sqrt{\left(\frac{\sinh(L/\xi)}{L/\xi}\right)^2 - 1}. \tag{D8}$$

We see again that the eigenvalue becomes independent of the momentum.

Thus, we see that, "in the large-system-size limit" means that, for the practical purpose of computing the EE away and close to the critical point, we may ignore the momentum dependence of the correlations. But since the diagonal basis is related to the laboratory frame by an OBC Fourier transform and two local-squeezing transformations that do not affect the entanglement, this means that the contribution to the entanglement in the GGE framework of a single mode is also the EE of a single spatial site. Thus the two results are equivalent.

Since we expect the GGE to hold for small system sizes $l/N \ll 1$, this extends our analytical results for the entanglement in this limit.

We will now show that a similar statement holds in the reciprocal phase.

b. Reciprocal phase

Recall the expressions for the correlations in the eigenbasis:

$$\overline{\langle \hat{b}_p^\dagger \hat{b}_p\rangle} = \frac{1}{2}\left(\cosh(2r_0)-1\right), \tag{D9}$$

$$\overline{\langle \hat{b}_{\bar{p}} \hat{b}_p\rangle} = \frac{1}{L}\sinh(2r_0)\,\frac{2p^2\left(1-e^{i\varphi L}\right)}{\varphi\left(4p^2-\varphi^2\right)}. \tag{D10}$$

The corresponding eigenvalue ν_p is given by

$$\nu_p = \sqrt{1+\sinh^2 2r_0\left(1-\frac{32p^4\left(1-\cos(\varphi L)\right)}{\left(\varphi L\left(4p^2-\varphi^2\right)\right)^2}\right)}. \tag{D11}$$

Away from the transition, φ is finite and, in the large-L limit, $\overline{\langle \hat{b}_{\bar{p}} \hat{b}_p\rangle} \approx 0$.

Close to the transition, $\varphi \to 0$. Taking $L \to \infty$ and keeping φL finite leads to

$$\overline{\langle \hat{b}_{\bar{p}} \hat{b}_p\rangle} \approx \frac{\sinh(2r_0)}{2}\,\frac{\left(1-e^{i\varphi L}\right)}{\varphi L}, \tag{D12}$$

which is again independent of p. We thus obtain that the GGE approach is equivalent to the minimal bipartition in the reciprocal phase as well.

2. Entanglement entropy and critical scaling

a. Nonreciprocal phase

In the nonreciprocal phase, the expression for ν_n is given by Eq. (D5).

Far from the critical point, we had $s(\nu_p) \approx \ln \nu_p \approx rN$ and thus

$$S_A = rlN, \tag{D13}$$

which leads to the supervolume-law scaling.

To get the scaling near the critical point, we consider the limit $L/\xi \ll 1$, which corresponds to a regime where the localization length is much greater than the system size. Expanding Eq. (D5) in powers of L/ξ leads to

$$\nu_p \approx N\frac{\Delta}{\sqrt{3}w}\left(1+\frac{1}{15}(L/\xi)^2\right) \tag{D14}$$

and

$$S_A \approx l\left(\ln N + \frac{1}{15}\frac{\Delta^2-g^2}{w^2}N^2\right). \tag{D15}$$

b. Reciprocal phase

The eigenvalue ν_p in the reciprocal phase is given by Eq. (D11).

Away from the transition, in the large-N limit, we have $\overline{\langle \hat{b}_{\bar{p}} \hat{b}_p\rangle} = 0$, so the EE is simply

$$S_A \approx ls\left(\cosh(2r_0)\right). \tag{D16}$$

Close to the transition, in the continuous limit, and for $\varphi L \ll 1$, we obtain

$$\nu_n \approx \frac{\Delta N}{\sqrt{3}w}\left(1+\frac{1}{15}(L/\xi)^2\right), \tag{D17}$$

which yields the same critical scaling as the nonreciprocal phase:

$$S_A \approx l\left(\ln N + \frac{1}{15}\frac{\Delta^2-g^2}{w^2}N^2\right). \tag{D18}$$

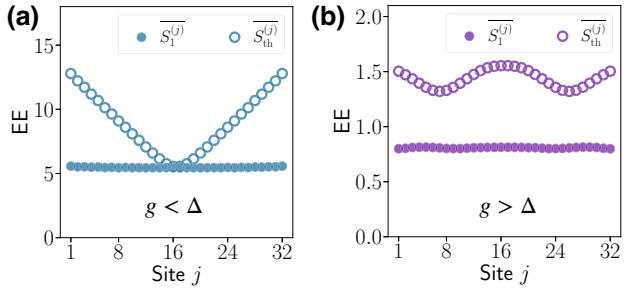

FIG. 7. A comparison of the expected thermal entropy $\overline{S_{\text{th}}^{(j)}}$ against the actual EE $\overline{S_1^{(j)}}$ for a chain of size $N = 32$ in (a) the nonreciprocal phase, with $w = 1$, $g = 0$, and $\Delta = 0.25$ and (b) the reciprocal phase, with $w = 1$, $g = 0.3$, and $\Delta = 0.25$.

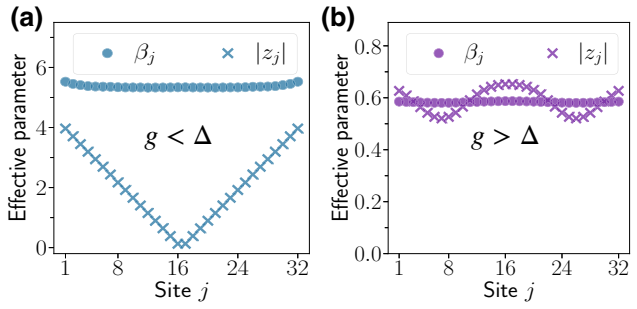

FIG. 8. A comparison of the local squeezing $|z_j|$ and local temperature $|\beta_j|$ for a chain of size $N = 32$ in (a) the nonreciprocal phase, with $w = 1$, $g = 0$, and $\Delta = 0.25$ and (b) the reciprocal phase, with $w = 1$, $g = 0.3$, and $\Delta = 0.25$.

APPENDIX E: LOCAL-SQUEEZING PLUS THERMAL-OCCUPATION ANSATZ

In this appendix, we show that simply considering the particle number is insufficient to fully characterize the spatial profile of entanglement.

Given only access to the density profile, what kind of EE profile might one expect such a system to have? One reasonable approach would be to think about the particle number as a proxy for the size of the local Hilbert space and, in general, we expect a larger local Hilbert space to indicate that the site is more entangled with the rest of the system. To make this concrete, suppose that a site j has occupation $\langle \hat{a}_j^\dagger \hat{a}_j \rangle$. One can try to associate an entropy with this density by assuming that when the system has thermalized, the density matrix of the site j will be approximately that of a thermal state, for which the EE is given by

$$S_{\text{th}}^{(j)} = (\langle \hat{a}_j^\dagger \hat{a}_j \rangle + 1)\ln(\langle \hat{a}_j^\dagger \hat{a}_j \rangle + 1) - \langle \hat{a}_j^\dagger \hat{a}_j \rangle \ln\langle \hat{a}_j^\dagger \hat{a}_j \rangle, \tag{E1}$$

and use this as an estimate for the actual EE $S_1^{(j)}$. We compare these two quantities by plotting their time-averaged values against each other in both the reciprocal and nonreciprocal phases (Fig. 7). In both cases, the true entanglement profile is flat up to finite-sized effects, whereas the expected thermal entropy reflects localization in the nonreciprocal case and periodic spatial oscillations in the reciprocal case. In both cases, the thermal entropy significantly overestimates the true EE.

Another way to appreciate the relationship between the particle number and entanglement is to explicitly extract the local squeezing and temperature of the time-averaged one-site density matrix. To do so, note that any diagonal single-site covariance matrix σ can be decomposed into a rotation followed by a squeezing operation on a thermal state:

$$\sigma = R \begin{pmatrix} e^z & 0 \\ 0 & e^{-z} \end{pmatrix} \begin{pmatrix} e^{2\beta} & 0 \\ 0 & e^{2\beta} \end{pmatrix} \begin{pmatrix} e^z & 0 \\ 0 & e^{-z} \end{pmatrix} R^T, \tag{E2}$$

where R is some orthogonal matrix and $e^{2\beta \pm 2z}$ are the eigenvalues of σ. The symplectic eigenvalue is entirely determined by β and the local-squeezing parameter z does not affect the entanglement properties at all. The quantities β and z can be easily obtained by diagonalizing σ.

In Fig. 8, we plot the values β_j, z_j extracted from the time-averaged covariance matrix σ_j at site j. These quantities display qualitatively similar features to the entropies of the previous plot, with the temperature being analogous to EE and the local squeezing displaying the same spatial distribution as the particle number. Notably, this allows us to make the more explicit statement that the spatial nonuniformity arising from nonreciprocity can be entirely characterized by local-squeezing operations, which do not affect the entanglement properties.

APPENDIX F: TWO ENABLING CLAIMS IN THE NONRECIPROCAL PHASE

1. The symplectic eigenvalue squared can be approximated using two-point correlators

In the main text, we have assumed that in the nonreciprocal phase,

$$\varepsilon_4 := \frac{\overline{(\langle \hat{d}^\dagger \hat{d} \rangle)^2} - \overline{\langle \hat{d}^\dagger \hat{d}^\dagger \rangle \langle \hat{d}\hat{d} \rangle}}{\left(\overline{\langle \hat{d}^\dagger \hat{d} \rangle}\right)^2 - \left(\overline{\langle \hat{d}^\dagger \hat{d}^\dagger \rangle}\right)\left(\overline{\langle \hat{d}\hat{d} \rangle}\right)} - 1 \sim O\left(\frac{1}{N}\right). \tag{F1}$$

To show this rigorously requires a long and tedious calculation, which we will outline here. We will show this in two limits: (1) deep in the nonreciprocal phase, where we fix r and take N to be large, and (2) near the critical point, where we fix N and take $g \to \Delta^-$.

First, let us set up the problem and classify various conserved quantities. For simplicity, we will pick $\hat{d}$ to be the operator on the first site of the chain, in the frame where $j_0 = (N+1)/2$ (picking any other site does not materially change the calculation, as we will see shortly). For brevity,

we will denote

$$t_s(x) := \sin\left(\frac{\pi x}{N+1}\right).$$

In this frame, the initial values of the momentum correlations are

$$\begin{aligned}\langle \hat{b}_k^\dagger \hat{b}_q\rangle_0 &= \frac{2}{N+1}\sum_{n=1}^{N} t_s(kn)t_s(qn)H(r,n,r_0),\\ \langle \hat{b}_k \hat{b}_q\rangle_0 &= \frac{2}{N+1}\sum_{n=1}^{N} t_s(kn)t_s(qn)G(r,n,r_0)(-1)^n,\end{aligned} \tag{F2}$$

where we have defined the quantities

$$\begin{aligned}H(r,n,r_0) &:= \frac{1}{2}\cosh\left(2r\left(n-\frac{N+1}{2}\right)\right)\cosh(2r_0)-\frac{1}{2},\\ G(r,n,r_0) &:= -\frac{1}{2}\sinh\left(2r\left(n-\frac{N+1}{2}\right)\right)\cosh(2r_0)\\ &\quad+\frac{i}{2}\sinh(2r_0),\end{aligned} \tag{F3}$$

associated with the initial real-space correlations in the tight-binding frame [see Eq. (C4)]. This gives the full time evolution of the four-point functions as

$$\begin{aligned}\langle \hat{d}^\dagger \hat{d}\rangle^2 &= \left(\frac{2}{N+1}\right)^2 \sum_{k,q,k',q'=1}^{N} t_s(q)t_s(q')t_s(k)t_s(k')\langle \hat{b}_q^\dagger \hat{b}_k\rangle_0 \langle \hat{b}_{q'}^\dagger \hat{b}_{k'}\rangle_0 e^{i(\varepsilon_q+\varepsilon_{q'}-\varepsilon_k-\varepsilon_{k'})t},\\ |\langle \hat{d}\hat{d}\rangle|^2 &= \left(\frac{2}{N+1}\right)^2 \sum_{k,q,k',q'=1}^{N} t_s(q)t_s(q')t_s(k)t_s(k')\langle \hat{b}_k \hat{b}_{k'}\rangle_0 \langle \hat{b}_q^\dagger \hat{b}_{q'}^\dagger\rangle_0 e^{i(\varepsilon_q+\varepsilon_{q'}-\varepsilon_k-\varepsilon_{k'})t},\end{aligned} \tag{F4}$$

where $\varepsilon_k = \sqrt{w^2+g^2-\Delta^2}\cos[\pi k/(N+1)]$.

To calculate the time average of the above quantities, we first observe that we can classify the conserved quantities into three sets, A, B, and C, defined by the conditions

$$\begin{aligned} A:&\quad q=k;&& q'=k',\\ B:&\quad q'=N+1-q;&& k'=N+1-k,\\ C:&\quad q=k';&& q'=k.\end{aligned} \tag{F5}$$

Note that for generic N, we always have this set of conserved quantities such that $\varepsilon_q+\varepsilon_{q'}-\varepsilon_k-\varepsilon_{k'}=0$. For a specific values of N, we can have other sets of conserved quantities associated with special values of the cosine but the effects of these do not scale with N, so we can ignore them.

We define the sum over the conserved quantities in each set by $I^r_{A,B,C}$ and $I^a_{A,B,C}$ for $\langle \hat{d}^\dagger \hat{d}\rangle_t^2$ and $|\langle \hat{d}\hat{d}\rangle_t|^2$, respectively, e.g.,

$$I_A^r := \left(\frac{2}{N+1}\right)^2 \sum_{k,q=1}^{N} t_s(q)^2 t_s(k)^2 \langle \hat{b}_q^\dagger \hat{b}_q\rangle_0 \langle \hat{b}_k^\dagger \hat{b}_k\rangle_0, \tag{F6}$$

and so forth. We note that these conserved quantities have some degeneracy between them, i.e., the sets A, B, and C have some overlap; e.g., A and B overlap when $q=k=N+1-k'=N+1-q'$. In the continuous limit, these overlaps disappear. However, for any finite N, they are responsible for the $O(1/N)$ correction observable in the numerics.

Finally, we observe that

$$\begin{aligned} I_A^r &= \left(\overline{\langle \hat{d}^\dagger \hat{d}\rangle_t}\right)^2,\\ I_B^a &= \left(\overline{\langle \hat{d}\hat{d}\rangle}\right)\left(\overline{\langle \hat{d}^\dagger \hat{d}^\dagger\rangle}\right)=0,\end{aligned} \tag{F7}$$

and

$$\begin{aligned} I_B^r &= I_C^r,\\ I_A^a &= I_C^a.\end{aligned} \tag{F8}$$

Hence, the time average of the four-point functions reduces to

$$\begin{aligned}\overline{\langle \hat{d}^\dagger \hat{d}\rangle_t^2} &= \left(\overline{\langle \hat{d}^\dagger \hat{d}\rangle_t}\right)^2 + 2I_B^r + O\left(\frac{1}{N}\left(\overline{\langle \hat{d}^\dagger \hat{d}\rangle^2}\right)\right),\\ \overline{|\langle \hat{d}\hat{d}\rangle|^2} &= 2I_A^a + O\left(\frac{1}{N}\left(\overline{|\langle \hat{d}\hat{d}\rangle|^2}\right)\right).\end{aligned} \tag{F9}$$

With the problem set up, we can now do some computation.

a. Large-N limit

First, note that in this case, $\left(\overline{\langle\hat{d}^\dagger\hat{d}\rangle_t}\right)^2 \sim O(e^{2Nr}/N^2)$. We simply need to show that the correction due to $I_B^r - I_A^a$ is negligible compared to $\left(\overline{\langle\hat{d}^\dagger\hat{d}\rangle_t}\right)^2$.

Generically, we might expect (and can show) that $I_B^r, I_A^a \sim O\left(e^{2Nr}/N^2\right)$. This means that $\left(\overline{\langle\hat{d}^\dagger\hat{d}\rangle_t}\right)^2$ would be a pretty bad approximation for $\overline{\langle\hat{d}^\dagger\hat{d}\rangle_t^2}$. Fortunately for us, it turns out that the differences will cancel in exactly the right way to allow us to make the desired approximation. First, let us write out the term in full:

$$\begin{aligned} &I_B^r - I_A^a \\ &= \left(\frac{2}{N+1}\right)^4 \sum_{k,q=1}^{N} t_s(q)^2 t_s(k)^2 \sum_{n,l=1}^{N} t_s(qn)t_s(ql)t_s(kn)t_s(kl)\left(H(r,l,r_0)H(r,n,r_0) - G(r,l,r_0)G^*(r,n,r_0)(-1)^{n+l}\right) \\ &= \left(\frac{2}{N+1}\right)^2 \sum_{n,l} A(n,l)A(n,l)\left(H(r,l,r_0)H(r,n,r_0) - G(r,l,r_0)G^*(r,n,r_0)(-1)^{n+l}\right), \end{aligned} \tag{F10}$$

where we have defined

$$A(n,l) = \frac{2}{N+1}\sum_{k=1}^{N} t_s(k)^2 t_s(kl)t_s(kn), \tag{F11}$$

which can be solved explicitly to obtain

$$A(n,l) = \begin{cases} \frac{1}{2} + \frac{1}{4}\delta_{n,1} + \frac{1}{4}\delta_{n,N}, & n = l, \\ -\frac{1}{4}, & |n-l| = 2, \\ 0, & \text{otherwise.} \end{cases} \tag{F12}$$

To show that $I_B^r - I_A^a$ is small, it suffices to pay attention only to the sum over $n = l$. Note that the $\delta_{n,1}$ and $\delta_{n,N}$ terms and the sum over $|n-l| = 2$ lead to a correction on the same order as the sum over $n = l$, as its contribution can be bounded by the former sum. Furthermore, the same calculation for sites other than the first site only change the condition to $|n-l| = 2k \mod (N+1)$, where k is the site number. Finally, we have

$$\begin{aligned} I_B^r - I_A^a &\sim \left(\frac{2}{N+1}\right)^2 \sum_{n=1}^{N}\left(H(r,n,r_0)^2 - |G(r,n,r_0)|^2\right) \\ &= \frac{1}{2}\left(\frac{2}{N+1}\right)^2 \sum_{n=1}^{N}(1 - \cosh(2r_0) \\ &\quad \cosh\left(2r\left(n - \frac{N+1}{2}\right)\right)\Big) \\ &= \frac{1}{2}\left(\frac{2}{N+1}\right)^2 \left(N - \cosh(2r_0)\frac{\sinh Nr}{\sinh r}\right) \\ &\sim O\left(\frac{1}{N^2}e^{Nr}\right). \end{aligned} \tag{F13}$$

With that, we conclude that

$$\begin{aligned} \overline{\langle\hat{d}^\dagger\hat{d}\rangle^2} - \overline{|\langle\hat{d}\hat{d}\rangle|^2} &= \left(\overline{\langle\hat{d}^\dagger\hat{d}\rangle_t}\right)^2 - \left(\overline{\langle\hat{d}\hat{d}\rangle}\right)\left(\overline{\langle\hat{d}^\dagger\hat{d}^\dagger\rangle}\right) \\ &\quad + O\left(\frac{1}{N}\left(\overline{\langle\hat{d}^\dagger\hat{d}\rangle^2} - \overline{|\langle\hat{d}\hat{d}\rangle|^2}\right)\right) \\ &= \left(1 + O\left(\frac{1}{N}\right)\right)\left(\left(\overline{\langle\hat{d}^\dagger\hat{d}\rangle_t}\right)^2 \right. \\ &\quad \left. - \left(\overline{\langle\hat{d}\hat{d}\rangle}\right)\left(\overline{\langle\hat{d}^\dagger\hat{d}^\dagger\rangle}\right)\right). \end{aligned} \tag{F14}$$

b. Near critical point

Near the critical point, we need to check what happens to $I_B^r - I_A^a$ when $g \to \Delta$. To investigate this limit, we first take $r \to 0$ and then express r and r_0 in terms of g, Δ, and w. Again, we only need to check the $n = l$ terms, with the other terms giving corrections of the same order. In this case, expanding in r and ignoring the parts that cancel with some R terms, Eq. (F13) becomes

$$\begin{aligned} I_B^r - I_A^a &\sim \frac{1}{3}N\cosh(2r_0)r^2 + O(r^3) \\ &\simeq O\left(N(\Delta^2 - g^2)/w^2\right), \end{aligned} \tag{F15}$$

which results in only a $O(1/N)$ correction to the calculation using the squares of two-point functions, which go as $N^2(\Delta^2 - g^2)/w^2$.

We note that the calculation proceeds almost identically on the reciprocal side of the critical point. For the reciprocal side, the term $\langle\hat{d}^\dagger\hat{d}\rangle^2$ does not oscillate at all and so does furnish any corrections to the symplectic eigenvalue, whereas the corrections from squaring the $|\langle\hat{d}\hat{d}\rangle|^2$ terms again goes as $O(1/N)$.

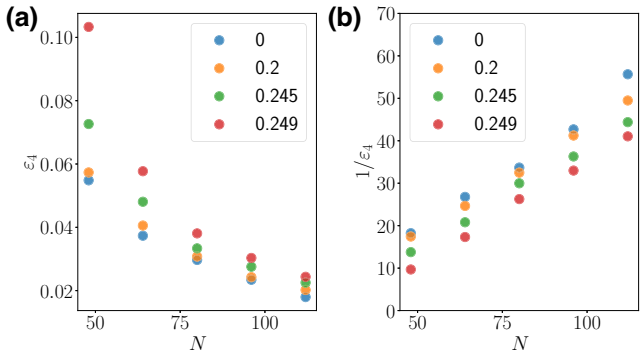

FIG. 9. (a) A plot of the quantity ε_4 defined in Eq. (F1) for $w = 1$, $\Delta = 0.25$, $g = 0$, 0.2, 0.245 and 0.249, and $N = 48$, 64, 80, 96, and 112. (b) A plot of $1/\varepsilon_4$ for the same parameters. The behavior is observed to be very close to linear with N, demonstrating that, indeed, $\varepsilon_4 \sim O(1/N)$.

To support these conclusions, In Fig. 9(a), we plot the numerically calculated values of ε_4 for the leftmost site and observe that it does indeed go away as N increases. We omit the $N = 16$ and $N = 32$ points, as they do not fall neatly into the large-N regime and we do not expect our assumptions to hold. In Fig. 9(b), we plot the inverse of the above quantity and observe that its behavior is indeed roughly linear with N.

2. Moving averages into the log only results in a small constant correction

Next, in the main text, we have also claimed that

$$\frac{\overline{\nu_t^4 - (\overline{\nu_t^2})^2}}{(\overline{\nu_t^2})^2} \sim O(1). \tag{F16}$$

This has allowed us to take $\overline{\ln \nu_t^2} \simeq \ln \overline{\nu_t^2}$, since $\ln \overline{\nu_t^2} \sim O(N)$. Now, ν_t^2 involves taking products of four two-point functions—we will simply sketch the main ideas.

First, note that the denominator goes as $O(e^{4Nr}/N^4)$. Now, for each selection rule arising from taking a product of two-point functions, one can take the most naive bound by simply taking absolute values of the summands and bounding the sine terms by 1. In that case, one can show that a product of four two-point functions goes at most as the number of selection rules multiplied by $O(e^{4Nr}/N^4)$ as well. Since the number of selection rules is independent of N, we can consider it a constant. As such, all factors of N in the numerator and denominator exactly cancel out.

In Fig. 10, we plot this quantity for the values of N and $g \leq 0.25$ studied in the main text and observe that, indeed, the correction to $\overline{\ln \nu_t^2}$ is exceedingly small compared to $\ln \overline{\nu_t^2}$ and approaches a constant for large N, as expected.

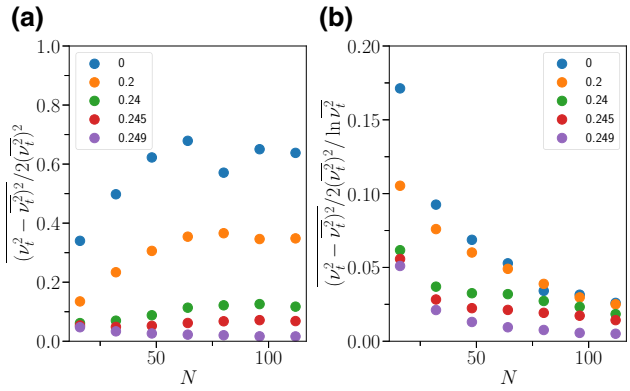

FIG. 10. (a) A plot of the first correction to the estimate $\overline{\ln \nu_t^2} \simeq \ln \overline{\nu_t^2}$ in the nonreciprocal phase, with $w = 1$, $\Delta = 0.25$, and $g = 0$, 0.2, 0.24, 0.245, and 0.249. We observe that it appears to plateau as N increases, consistent with the assumptions in the main text. (b) A plot of the first correction relative to the value of $\ln \overline{\nu_t^2}$, with the same parameters as in (a). We observe that the relative size of the correction appears to go to zero for large N.

[1] X. Cao, A. Tilloy, and A. D. Luca, Entanglement in a fermion chain under continuous monitoring, SciPost Phys. **7**, 024 (2019).

[2] B. Skinner, J. Ruhman, and A. Nahum, Measurement-induced phase transitions in the dynamics of entanglement, Phys. Rev. X **9**, 031009 (2019).

[3] Y. Li, X. Chen, and M. P. A. Fisher, Quantum Zeno effect and the many-body entanglement transition, Phys. Rev. B **98**, 205136 (2018).

[4] M. J. Gullans, S. Krastanov, D. A. Huse, L. Jiang, and S. T. Flammia, Quantum coding with low-depth random circuits, Phys. Rev. X **11**, 031066 (2021).

[5] Y. Bao, S. Choi, and E. Altman, Theory of the phase transition in random unitary circuits with measurements, Phys. Rev. B **101**, 104301 (2020).

[6] S. Choi, Y. Bao, X.-L. Qi, and E. Altman, Quantum error correction in scrambling dynamics and measurement-induced phase transition, Phys. Rev. Lett. **125**, 030505 (2020).

[7] O. Alberton, M. Buchhold, and S. Diehl, Entanglement transition in a monitored free-fermion chain: From extended criticality to area law, Phys. Rev. Lett. **126**, 170602 (2021).

[8] A. C. Potter and R. Vasseur, in *Quantum Science and Technology* (Springer International Publishing, Cham, Switzerland, 2022), p. 211.

[9] M. P. Fisher, V. Khemani, A. Nahum, and S. Vijay, Random quantum circuits, Annu. Rev. Condens. Matter Phys. **14**, 335 (2023).

[10] C.-M. Jian, Y.-Z. You, R. Vasseur, and A. W. W. Ludwig, Measurement-induced criticality in random quantum circuits, Phys. Rev. B **101**, 104302 (2020).

[11] M. Buchhold, Y. Minoguchi, A. Altland, and S. Diehl, Effective theory for the measurement-induced phase transition of Dirac fermions, Phys. Rev. X **11**, 041004 (2021).

[12] X. Turkeshi, A. Biella, R. Fazio, M. Dalmonte, and M. Schiró, Measurement-induced entanglement transitions in the quantum Ising chain: From infinite to zero clicks, Phys. Rev. B **103**, 224210 (2021).

[13] X. Turkeshi, R. Fazio, and M. Dalmonte, Measurement-induced criticality in $(2+1)$-dimensional hybrid quantum circuits, Phys. Rev. B **102**, 014315 (2020).

[14] T. Jin and D. G. Martin, Kardar-Parisi-Zhang physics and phase transition in a classical single random walker under continuous measurement, Phys. Rev. Lett. **129**, 260603 (2022).

[15] M. Fava, L. Piroli, T. Swann, D. Bernard, and A. Nahum, Nonlinear sigma models for monitored dynamics of free fermions, ArXiv:2302.12820 (2023).

[16] C.-M. Jian, H. Shapourian, B. Bauer, and A. W. W. Ludwig, Measurement-induced entanglement transitions in quantum circuits of non-interacting fermions: Born-rule versus forced measurements, ArXiv:2302.09094 (2023).

[17] I. Poboiko, P. Pöpperl, I. V. Gornyi, and A. D. Mirlin, Theory of free fermions under random projective measurements, ArXiv:2304.03138 (2023).

[18] J. M. Koh, S.-N. Sun, M. Motta, and A. J. Minnich, Measurement-induced entanglement phase transition on a superconducting quantum processor with mid-circuit readout, Nat. Phys. **19**, 1314 (2023).

[19] M. J. Gullans and D. A. Huse, Scalable probes of measurement-induced criticality, Phys. Rev. Lett. **125**, 070606 (2020).

[20] M. Ippoliti and V. Khemani, Postselection-free entanglement dynamics via spacetime duality, Phys. Rev. Lett. **126**, 060501 (2021).

[21] C. Noel, P. Niroula, D. Zhu, A. Risinger, L. Egan, D. Biswas, M. Cetina, A. V. Gorshkov, M. J. Gullans, D. A. Huse, and C. Monroe, Measurement-induced quantum phases realized in a trapped-ion quantum computer, Nat. Phys. **18**, 760 (2022).

[22] T. Iadecola, S. Ganeshan, J. H. Pixley, and J. H. Wilson, Dynamical entanglement transition in the probabilistic control of chaos, Preprint ArXiv:2207.12415 (2022).

[23] M. Buchhold, T. Müller, and S. Diehl, Revealing measurement-induced phase transitions by pre-selection, ArXiv:2208.10506 (2022).

[24] Y. Li, Y. Zou, P. Glorioso, E. Altman, and M. P. A. Fisher, Cross entropy benchmark for measurement-induced phase transitions, Preprint ArXiv:2209.00609 (2022).

[25] H. Dehghani, A. Lavasani, M. Hafezi, and M. J. Gullans, Neural-network decoders for measurement induced phase transitions, Preprint ArXiv:2204.10904 (2022).

[26] G. Passarelli, X. Turkeshi, A. Russomanno, P. Lucignano, M. Schiró, and R. Fazio, Post-selection-free measurement-induced phase transition in driven atomic gases with collective decay, ArXiv:2306.00841 (2023).

[27] J. C. Hoke, M. Ippoliti, D. Abanin, R. Acharya, M. Ansmann, F. Arute, K. Arya, A. Asfaw, J. Atalaya, and J. C. Bardin, *et al.*, Quantum information phases in space-time: Measurement-induced entanglement and teleportation on a noisy quantum processor, ArXiv:2303.04792 (2023).

[28] Y. L. Gal, X. Turkeshi, and M. Schiró, Volume-to-area law entanglement transition in a non-Hermitian free fermionic chain, SciPost Phys. **14**, 138 (2023).

[29] K. Kawabata, T. Numasawa, and S. Ryu, Entanglement phase transition induced by the non-Hermitian skin effect, Phys. Rev. X **13**, 021007 (2023).

[30] S. Gopalakrishnan and M. J. Gullans, Entanglement and purification transitions in non-Hermitian quantum mechanics, Phys. Rev. Lett. **126**, 170503 (2021).

[31] X. Turkeshi and M. Schiró, Entanglement and correlation spreading in non-Hermitian spin chains, Phys. Rev. B **107**, L020403 (2023).

[32] N. Hatano and D. R. Nelson, Localization transitions in non-Hermitian quantum mechanics, Phys. Rev. Lett. **77**, 570 (1996).

[33] N. Hatano and D. R. Nelson, Vortex pinning and non-Hermitian quantum mechanics, Phys. Rev. B **56**, 8651 (1997).

[34] S. Yao, F. Song, and Z. Wang, Non-Hermitian Chern bands, Phys. Rev. Lett. **121**, 136802 (2018).

[35] V. M. Martinez Alvarez, J. E. Barrios Vargas, and L. E. F. Foa Torres, Non-Hermitian robust edge states in one dimension: Anomalous localization and eigenspace condensation at exceptional points, Phys. Rev. B **97**, 121401 (2018).

[36] F. K. Kunst, E. Edvardsson, J. C. Budich, and E. J. Bergholtz, Biorthogonal bulk-boundary correspondence in non-Hermitian systems, Phys. Rev. Lett. **121**, 026808 (2018).

[37] A. McDonald, T. Pereg-Barnea, and A. A. Clerk, Phase-dependent chiral transport and effective non-Hermitian dynamics in a bosonic Kitaev-Majorana chain, Phys. Rev. X **8**, 041031 (2018).

[38] N. Okuma and M. Sato, Non-Hermitian topological phenomena: A review, ArXiv:2205.10379 (2022).

[39] Y. Ashida, Z. Gong, and M. Ueda, Non-Hermitian physics, Adv. Phys. **69**, 249 (2020).

[40] E. J. Bergholtz, J. C. Budich, and F. K. Kunst, Exceptional topology of non-Hermitian systems, Rev. Mod. Phys. **93**, 015005 (2021).

[41] R. Lin, T. Tai, L. Li, and C. H. Lee, Topological non-Hermitian skin effect, Front. Phys. **18**, 53605 (2023).

[42] Y.-X. Wang and A. A. Clerk, Non-Hermitian dynamics without dissipation in quantum systems, Phys. Rev. A **99**, 063834 (2019).

[43] J. del Pino, J. J. Slim, and E. Verhagen, Non-Hermitian chiral phononics through optomechanically induced squeezing, Nature **606**, 82 (2022).

[44] C. C. Wanjura, J. J. Slim, J. del Pino, M. Brunelli, E. Verhagen, and A. Nunnenkamp, Quadrature nonreciprocity in bosonic networks without breaking time-reversal symmetry, Nat. Phys. **19**, 1429 (2023).

[45] T. Zhou and X. Chen, Nonunitary entanglement dynamics in continuous-variable systems, Phys. Rev. B **104**, L180301 (2021).

[46] Y. Minoguchi, P. Rabl, and M. Buchhold, Continuous Gaussian measurements of the free boson CFT: A model for exactly solvable and detectable measurement-induced dynamics, SciPost Phys. **12**, 009 (2022).

[47] For $w < \Delta$, both the OBC and the PBC case become unstable.

[48] K. Kawabata, K. Shiozaki, M. Ueda, and M. Sato, Symmetry and topology in non-Hermitian physics, Phys. Rev. X **9**, 041015 (2019).
[49] L. Hackl and E. Bianchi, Bosonic and fermionic Gaussian states from Kähler structures, SciPost Phys. Core **4**, 025 (2021).
[50] P. Calabrese and J. Cardy, Evolution of entanglement entropy in one-dimensional systems, J. Stat. Mech.: Theory Exp. **2005**, P04010 (2005).
[51] C. Weedbrook, S. Pirandola, R. García-Patrón, N. J. Cerf, T. C. Ralph, J. H. Shapiro, and S. Lloyd, Gaussian quantum information, Rev. Mod. Phys. **84**, 621 (2012).
[52] A. Serafini, *Quantum Continuous Variables: A Primer of Theoretical Methods* (CRC Press, Boca Raton FL, 2023).
[53] D. N. Page, Information in black hole radiation, Phys. Rev. Lett. **71**, 3743 (1993).
[54] M. Fagotti and P. Calabrese, Evolution of entanglement entropy following a quantum quench: Analytic results for the *xy* chain in a transverse magnetic field, Phys. Rev. A **78**, 010306 (2008).
[55] V. Alba and P. Calabrese, Entanglement and thermodynamics after a quantum quench in integrable systems, Proc. Natl. Acad. Sci. **114**, 7947 (2017).
[56] G. Parez, R. Bonsignori, and P. Calabrese, Exact quench dynamics of symmetry resolved entanglement in a free fermion chain, J. Stat. Mech.: Theory Exp. **2021**, eid 093102 (2021).
[57] M. Rigol, V. Dunjko, V. Yurovsky, and M. Olshanii, Relaxation in a completely integrable many-body quantum system: An *ab initio* study of the dynamics of the highly excited states of 1D lattice hard-core bosons, Phys. Rev. Lett. **98**, 050405 (2007).
[58] L. Vidmar and M. Rigol, Generalized Gibbs ensemble in integrable lattice models, J. Stat. Mech.: Theory Exp. **6**, 064007 (2016).
[59] V. Alba and P. Calabrese, Entanglement dynamics after quantum quenches in generic integrable systems, SciPost Phys. **4**, 017 (2018).
[60] Y. Minoguchi, P. Rabl, and M. Buchhold, Continuous Gaussian measurements of the free boson CFT: A model for exactly solvable and detectable measurement-induced dynamics, SciPost Phys. **12**, 009 (2022).
[61] X. Chen, Y. Li, M. P. A. Fisher, and A. Lucas, Emergent conformal symmetry in nonunitary random dynamics of free fermions, Phys. Rev. Res. **2**, 033017 (2020).
[62] X. Jia, A. R. Subramaniam, I. A. Gruzberg, and S. Chakravarty, Entanglement entropy and multifractality at localization transitions, Phys. Rev. B **77**, 014208 (2008).
[63] J. H. Bardarson, F. Pollmann, and J. E. Moore, Unbounded growth of entanglement in models of many-body localization, Phys. Rev. Lett. **109**, 017202 (2012).
[64] M. J. Gullans and D. A. Huse, Localization as an entanglement phase transition in boundary-driven anderson models, Phys. Rev. Lett. **123**, 110601 (2019).